Minimal Partitions for p-norms of eigenvalues

Beniamin Bogosel, Virginie Bonnaillie-Noël

MINIMAL PARTITIONS FOR p-NORMS OF EIGENVALUES

B. BOGOSEL AND V. BONNAILLIE-NOËL

Abstract. In this article we are interested in studying partitions of the square, the disk and the equilateral triangle which minimize a p-norm of eigenvalues of the Dirichlet-Laplace operator. The extremal case of the infinity norm, where we minimize the largest fundamental eigenvalue of each cell, is one of our main interests. We propose three numerical algorithms which approximate the optimal configurations and we obtain tight upper bounds for the energy, which are better than the ones given by theoretical results. A thorough comparison of the results obtained by the three methods is given. We also investigate the behavior of the minimal partitions with respect to p. This allows us to see when partitions minimizing the 1-norm and the infinity-norm are different.

1. Introduction

1.1. **Motivation.** In this paper we are interested in determining minimal partitions for some cost functionals where is involved the p-norm of some spectral quantities (p is a positive integer or $p = \infty$).

Let Ω be a bounded domain in $\mathbb{R}^2$ with piecewise-$\mathcal{C}^1$ boundary and k be a positive integer $k \geq 1$. For any domain $D \subset \Omega$, $(\lambda_j(D))_{j\geq 1}$ denotes the eigenvalues of the Laplace operator on D with Dirichlet boundary conditions, arranged in non decreasing order and repeated with multiplicity.

We denote by $\mathfrak{P}_k(\Omega)$ the set of k-partitions $\mathcal{D} = (D_1, \dots, D_k)$ such that

- $(D_j)_{1\leq j\leq k}$ are connected, open and mutually disjoint subsets of Ω,
- $\mathrm{Int}(\bigcup_{1\leq j\leq k} \overline{D_j}) \setminus \partial\Omega = \Omega$.

For any k-partition $\mathcal{D} \in \mathfrak{P}_k(\Omega)$, we define the *$p$-energy* by

$$\Lambda_{k,p}(\mathcal{D}) = \left(\frac{1}{k}\sum_{i=1}^{k} \lambda_1(D_i)^p\right)^{1/p}, \qquad \forall p \geq 1. \tag{1.1}$$

By extension, if we consider the infinite norm, we define the *energy* of $\mathcal{D}$ by

$$\Lambda_{k,\infty}(\mathcal{D}) = \max_{1\leq i\leq k} \lambda_1(D_i). \tag{1.2}$$

With a little abuse of notation, we notice that

$$\Lambda_{k,p}(\mathcal{D}) = \frac{1}{k^{1/p}} \Big\| \big(\lambda_1(D_1), \dots, \lambda_1(D_k)\big) \Big\|_p.$$

The index ∞ is omitted when there is no confusion. The optimal problem we consider is to determine the infimum of the p-energy ($1 \leq p \leq \infty$) among the partitions of $\mathfrak{P}_k(\Omega)$:

$$\mathfrak{L}_{k,p}(\Omega) = \inf_{\mathcal{D}\in\mathfrak{P}_k(\Omega)} \Lambda_{k,p}(\mathcal{D}), \qquad \forall 1 \leq p \leq \infty, \quad \forall k \geq 1. \tag{1.3}$$

A partition $\mathcal{D}^*$ such that $\Lambda_{k,p}(\mathcal{D}^*) = \mathfrak{L}_{k,p}(\Omega)$ is called a p-minimal k-partition of Ω.

This optimization problem has been a subject of great interest in the last couple of years [14, 13, 15, 23]. Two cases are especially studied: the sum which corresponds to $p = 1$ and the max, corresponding to $p = \infty$. These problems are considered from a theoretical point of view in [14, 15, 16, 17, 23], where some existence and regularity results are obtained. The numerical study of this problem is also important in order to exhibit some candidates as

Date: December 19, 2016.

optimal partitions (see [12] for $p = 1$ and [8, 5, 9, 10, 23] for $p = \infty$). More recently, the link between these two optimization problems is taken into consideration in [22]. In particular, a criterion is established to assert that a ∞-minimal k-partition is not a 1-minimal k-partition.

We start by stating the following existence result.

Theorem 1.1. *For any $k \geq 1$ and $p \in [1, +\infty]$, there exists a regular p-minimal k-partition.*

Let us recall that a k-partition $\mathcal{D}$ is called *regular* if its boundary, $N(\mathcal{D}) = \cup_{1 \leq i \leq k} \partial D_i$, is locally a regular curve, except at a finite number of singular points, where a finite number of half-curves meet with equal angles. We say that $\mathcal{D}$ satisfies the *equal angle meeting property*.

In the case $k = 1$, if Ω is connected, then the p-minimal 1-partition is Ω itself, for any p. From now, we will consider $k \geq 2$.

Remark 1.2. Note that if we relax the condition $\mathrm{Int}(\bigcup_{1 \leq j \leq k} \overline{D_j}) \setminus \partial\Omega = \Omega$ and consider the optimization problem among partitions such that we have only an inclusion

$$\mathrm{Int}\Big(\bigcup_{1 \leq j \leq k} \overline{D_j} \Big) \setminus \partial\Omega \subset \Omega, \tag{1.4}$$

Theorem 1.1 is still available and any p-minimal k-partitions is strong (this means we have equality in (1.4)).

1.2. **Main results and organisation of the paper.** In Section 2 we present the iterative algorithm for the optimization of the p-norm based on the results of [12]. The implementation produces different behaviors when we consider the minimization problem for $p = 1$ or $p = \infty$. In Section 3 we recall some theoretical aspects needed in order to analyze our numerical results and also to propose more efficient algorithms.

Next, in Section 4 we concentrate on the case of the ∞-minimal partitions. We describe a new iterative method based on a penalization of the difference of the eigenvalues and the mixed Dirichlet-Neumann approach where we restrict ourselves to nodal partitions of a mixed problem. Here we compare the three methods and exhibit better upper bounds for $\mathfrak{L}_{k,\infty}(\Omega)$. At the end of this section, we prove that almost all of the candidates to be ∞-minimal k-partition can not be optimal for the sum, in coherence with theoretical results of [22].

In Section 5 we analyze the behavior of the optimal partitions for the p-norm with respect to p by looking at the evolution of the associated energies and the partitions. More precisely, when $2 \leq k \leq 10$, numerical simulations for the square, the disk or the equilateral triangle suggest that the energy $\mathfrak{L}_{k,p}(\Omega)$ is strictly increasing with p except in the following cases:

Conjecture 1.3. *The energy $\mathfrak{L}_{k,p}(\Omega)$ is constant with respect to p when*

- *Ω is a disk and $k \in \{2, 3, 4, 5\}$,*
- *Ω is a square and $k \in \{2, 4\}$,*
- *Ω is an equilateral triangle and k is a triangular number, that is to say of the form $n(n+1)/2$ with $n \geq 2$.*

In these cases, there exists a k-partition which is p-minimal for any $p \in [1, +\infty]$.

- *For the disk, this partition is composed of k angular sectors of opening $2\pi/k$ (see Figure 2).*
- *A minimal 2-partition for the square is given by two equal rectangles or two equal triangles with right angle (see Figure 4(a)). For the square and $k = 4$ the minimal partition is composed of 4 squares (see Figure 4(b)).*
- *For the equilateral triangle the minimal k-partition seems to consist of 3 equal quadrilaterals, $3(n-2)$ pentagons and $(n-2)(n-3)/2$ regular hexagons (see Figures 6(a) and 21).*

2. Numerical iterative algorithm

2.1. **Numerical method for the sum.** The problem of minimizing numerically the sum of the first eigenvalues of the Dirichlet-Laplace operator corresponding to a partition of a planar domain Ω has been studied numerically by Bourdin, Bucur and Oudet in [12]. In order to simplify the computation and the representation of the partition they represented each cell of the partition as a discrete function on a fixed finite differences grid. It is possible to compute the first eigenvalue of a subset D of Ω by using a relaxed formulation of the problem based on [19]. If φ is a function which approximates χ_D, the characteristic function of D, then we consider the problem

$$-\Delta u + C(1-\varphi)u = \lambda_j(C,\varphi)u \qquad \text{in } \Omega, \tag{2.1}$$

with $C \gg 1$. In the case where $\varphi = \chi_D$ it is proved that $\lambda_j(C,\varphi) \to \lambda_j(D)$ as $C \to \infty$. Moreover, in [4] the following quantitative estimation of the rate of convergence is given: if $\varphi = \chi_D$ then

$$\frac{|\lambda_j(D) - \lambda_j(C,\varphi)|}{\lambda_j(D)} = O(C^{-1/6}).$$

From now on, we only deal with the first eigenvalue. As a consequence of the quantitative estimation given above, it is desirable to have a penalization constant C as large as possible in our computations, in order to obtain a good approximation of the eigenvalues. The discretization of the problem (2.1) is straightforward if we consider a finite differences grid. We consider a square bounding box containing the domain Ω. On this box we construct a $N \times N$ uniform grid and we approximate the Laplacian of u using centered finite differences. This allows us to write a discrete version of problem (2.1) in the following matrix form

$$(A + \operatorname{diag}(C(1-\tilde{\varphi}))\tilde{u} = \lambda_1(C,\tilde{\varphi})\tilde{u}, \tag{2.2}$$

where the matrix A is the discrete Laplacian on the finite differences grid and $\tilde{u}$ a column vector. The matrices involved in the discrete form of the problem (2.2) are sparse and thus the problem can be solved efficiently in Matlab using `eigs`. We note here that the domain Ω does not need to fill the whole bounding box and that imposing that the functions φ are zero on the nodes outside Ω automatically adds a penalization factor on these nodes. In this way we can study various geometries, like the disk and the equilateral triangle, while still working on a finite-difference grid on a square bounding box.

Remark 2.1. Finite element formulations are also possible and we refer to [4] for a brief presentation. One drawback is that if we consider finite elements then the discrete problem analogue to (2.2) is a generalized eigenvalue problem. The computational cost in this case is higher and this prevents us from being able to work with fine discretizations.

In our numerical study of optimal partitioning problems in connection to spectral quantities we use the approach described above to represent the cells and to compute the eigenvalues. We replace each set D_j by a discrete density function $\tilde{\varphi}_j : \Omega \to [0,1]$ and use the formulation (2.1) and its discrete form (2.2) to compute an approximation of $\lambda_1(D_j)$. The condition that the sets $(D_j)_{1\le j\le k}$ form a partition of the domain Ω can be implemented by imposing that the densities $\tilde{\varphi}_j$ associated to D_j have sum equal to one:

$$\sum_{j=1}^{k} \tilde{\varphi}_j = 1.$$

In order to have an efficient optimization algorithm we use a gradient based approach. For this we compute the gradient of $\lambda_1(C,\tilde{\varphi})$ with respect to each node of the grid and, as in [12], we get

$$\partial_i \lambda_1(C,\tilde{\varphi}) = -C\tilde{u}_i^2, \qquad i,j = 1,\dots,N.$$

2.2. **Adaptation for the p-norm.** As we see in Introduction, we are not only interesting in the optimization problem for the sum (see (1.1) with $p = 1$) but also for any p-norm and one of our objectives is to study numerically the minimizers of the quantity

$$\max_{1\leq j\leq k} \lambda_1(D_j). \tag{2.3}$$

This functional is non-smooth and therefore we cannot minimize it directly. One way to approach minimizers of (2.3) has been proposed in [10] and it consists in minimizing instead the p-norms $\Lambda_{k,p}(\mathcal{D})$ defined in (1.1), for large p: It is clear that as $p \to \infty$ these p-norms $\Lambda_{k,p}(\mathcal{D})$ converge to the largest eigenvalue among $\{\lambda_1(D_j),\ 1 \leq j \leq k\}$. In order to optimize $\Lambda_{k,p}(\mathcal{D})$ we modify the expression of the gradient in the algorithm presented in [12] by adding a factor corresponding to the derivative of the p-norm

$$\partial_i \Lambda_{k,p}(\mathcal{D}) = \frac{1}{pk} \left(\frac{1}{k} \sum_{j=1}^{k} \lambda_1(C, \tilde{\varphi}_j)^p \right)^{1/p-1} \times \left(\sum_{j=1}^{k} \partial_i \lambda_1(C, \tilde{\varphi}_j) \right).$$

2.3. **Grid restriction procedure.** We perform the optimization starting from random admissible densities on a 60×60 grid on the square bounding box. In order to have a more precise description of the contours we perform a few successive refinements by doubling the number of discretization points in both horizontal and vertical directions, until we reach a 480×480 grid. More precisely, given a grid size, we apply a gradient descent algorithm using the expression of the gradient of the eigenvalue given in the previous subsection. At each iteration, after the update of the functions $\tilde{\varphi}_j$ we project them on the constraint condition by replacing each function $\tilde{\varphi}_j$ by $|\tilde{\varphi}_j|/(\sum_{i=1}^{k} |\tilde{\varphi}_i|)$. This projection algorithm is the same as the one suggested in [12]. We stop when the value of the p-norm does not decrease when considering a step length of at least 10^{-6}. Once we obtain a numerical solution on a given grid we use an interpolation procedure to pass to a denser grid. Then we restart the gradient descent algorithm on this new grid starting from the interpolated partition. We stop when we reach a grid of the desired size, in our case 480×480. We notice that on the 480×480 grid we cannot use a penalization parameter C which is greater than 10^4, since the matrix $A + \mathrm{diag}(C(1 - \tilde{\varphi}))$ becomes ill conditioned. Indeed, we can see that a large part of the grid is not really used in the computation of the eigenvalue, since, in most cases, roughly N^2/k of the points of the grid are covered by the support of $\tilde{\varphi}_j$ (which should converge to some subdomain D_j of a minimal k-partition). In order to surpass this problem and to be able to increase the parameter C we propose the following modification of the algorithm used in [12].

The initial densities are chosen randomly and projected onto the constraint like shown in [12]. At each iteration of the gradient method, we look for the points of the grid which satisfy $\tilde{\varphi}_j > 0.01$ (represented with dark blue in Figure 1) and then we compute the smallest rectangular region of the grid which contains these points (represented with red in Figure 1). As you can see in Figure 1 the first two situations correspond to cases where the cell function $\tilde{\varphi}_j$ is not localized. On the other hand, from the moment when the cell is concentrated on only one part of the partitioned region Ω the rectangular neighborhood is much smaller and the amount of points where we need to impose the penalization is diminished. The points where the penalization is imposed are represented with cyan in Figure 1. Note that in order to allow the cells to interact we extend the rectangular neighborhood with at least 5 rows/columns (if contained in Ω). In order to keep the advantage of working on a fixed computation grid, we set the cell's discrete values and gradient equal to zero on the points outside the local rectangular grid. This is natural, since cells which are far away do not have great impact on the dynamic of the current cell. Note that this procedure does not restrict the movement of the cells since these rectangular neighborhoods are dynamically computed at each iteration. Since the number of points on which we impose the penalization is significantly decreased the discrete problem remains well posed even for larger values of

C of order 10^7. Figure 1 represents the evolution of the set $\{\tilde{\varphi}_7 > 0.01\}$ and so of the local grid after 1, 10, 25, 45 and 85 iterations of the gradient method when we implement the algorithm with $k = 10$ and $p = 1$. Here, we have not yet done any refinment of the grid.

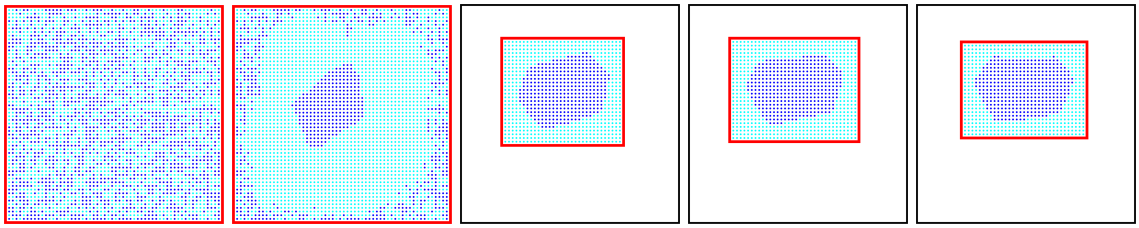

FIGURE 1. Evolution of the local grid for a cell for iterations $1, 10, 25, 45, 85$. This computation corresponds to $k = 10$ and $p = 1$.

The optimization procedure described above uses a relaxed formulation. Let us now describe how this allows to construct a partition $\mathcal{D}^{k,p}$ of Ω whose energy will be computed with a finite element method.

- For each $i \in \{1, \dots, k\}$ we look for the grid points where $\tilde{\varphi}_i \geq \tilde{\varphi}_j$ for every $j \neq i$.
- We use Matlab's `contour` function to find the contour associated to these points.

This approach, as opposed to looking directly at some level sets of $\tilde{\varphi}$, has the advantage that the contours we obtain form a strong partition $\mathcal{D}^{k,p}$ of the domain Ω. Then we compute the first Dirichlet-Laplacian eigenvalue on each subdomain of the partition by using a finite element method : either each cell is then triangulated using the free software Triangle [27] and its Dirichlet-Laplacian eigenvalues are computed using the finite elements library MÉLINA [25], or we use FREEFEM++ [20]. In cases where both MÉLINA and FREEFEM++ are used we recover the same results.

2.4. **Numerical results.** We denote by $\mathcal{D}^{k,p}$ the partition obtained by the iterative numerical method. We study three particular geometries of Ω: a square $\square$ of sidelength 1, a disk $\bigcirc$ of radius 1 and an equilateral triangle $\triangle$ of sidelength 1. We perform computations up to $p = 50$ and we hope that the partitions obtained numerically for $p = 50$ are good candidates to approximate the ∞-minimal k-partition.

Let us first consider the case of the disk. When $k = 2, 3, 4, 5$, the algorithm gives the same partition for the two optimization problems (the sum $p = 1$ and the max $p = \infty$). These partitions, given in Figure 2, are composed of k similar angular sectors of opening $2\pi/k$ and then, the first eigenvalues on each cell are equal. Some comments about the relation to the notion of equipartition will be addressed in the next section. It is conjectured that the "Mercedes partition" is minimal for the max, but this result is not yet proved (see [21, 6]). These simulations reinforce this conjecture.

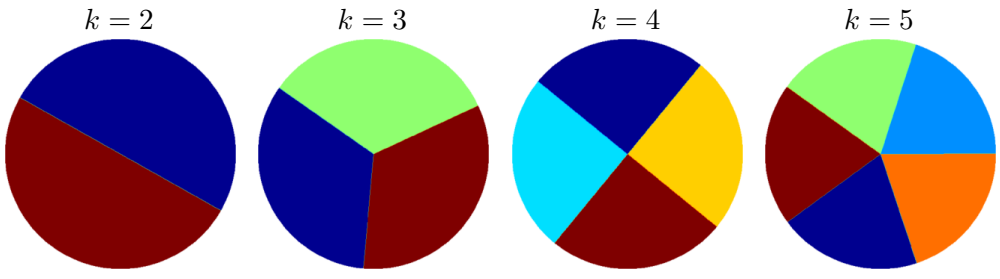

FIGURE 2. Candidates for p-minimal k-partitions of the disk for $p = 1$ and 50.

We illustrate in Figure 3 the results obtained for $p = 1, 50$ and $k \in \{2, 3, 4, 5\}$ in the case of the equilateral triangle. Note that except for $k = 4$, partitions do not change much

their structure. The case $k = 4$ for the equilateral triangle is one of the few cases where the topology of the partition changes significantly with p, approaching the partition into 4 equal triangles as p is increasing. In Table 1, we analyze the energies of the numerical

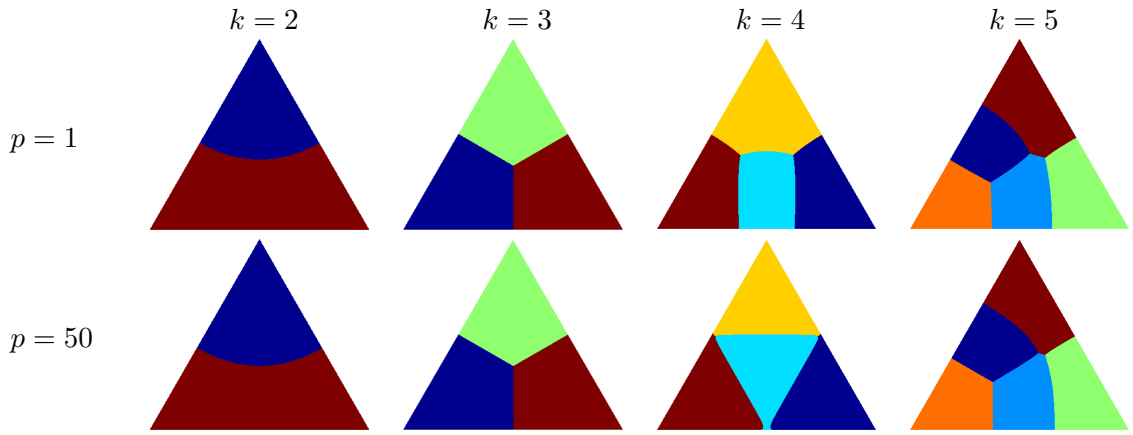

FIGURE 3. Candidates for p-minimal k-partitions of the equilateral triangle when $p = 1$ and 50.

p-minimal k-partitions for $p = 1, 50$. For each partition, we give the energy $\Lambda_{k,p}(\mathcal{D}^{k,p})$ (which corresponds to the energy for which $\mathcal{D}^{k,p}$ should be optimal) and the largest first eigenvalue on the cells of $\mathcal{D}^{k,p}$, that is to say $\Lambda_{k,\infty}(\mathcal{D}^{k,p})$. We can observe that the minimizer for $p = 1$ has a larger maximal eigenvalue than the one obtained for $p = 50$. This indicates that partitions $\mathcal{D}^{k,1}$ which minimize $\Lambda_{k,1}$ are not necessarily good candidates for minimizing $\Lambda_{k,\infty}$ and that the candidates $\mathcal{D}^{k,50}$ give better upper bound for $\mathfrak{L}_{k,\infty}(\Omega)$ than the candidates $\mathcal{D}^{k,1}$. Indeed, we observe that

$$\Lambda_{k,\infty}(\mathcal{D}^{k,50}) \leq \Lambda_{k,\infty}(\mathcal{D}^{k,1}), \qquad 2 \leq k \leq 5.$$

Furthermore, by definition of $\mathfrak{L}_{k,\infty}(\triangle)$, we have $\mathfrak{L}_{k,\infty}(\triangle) \leq \Lambda_{k,\infty}(\mathcal{D}^{k,50})$ for any k. In the case $p = 50$, the energies $\Lambda_{k,50}$ and $\Lambda_{k,\infty}$ are rather close, which leads one to believe that the numerical p-minimal k-partition with $p = 50$ is a rather good candidate to minimize the maximum of the first eigenvalues $\Lambda_{k,\infty}$.

	$\mathcal{D}^{k,1}$		$\mathcal{D}^{k,50}$	
k	$\Lambda_{k,1}$	$\Lambda_{k,\infty}$	$\Lambda_{k,50}$	$\Lambda_{k,\infty}$
2	106.62	136.11	123.25	123.38
3	143.05	143.07	143.06	143.07
4	206.15	229.44	209.86	211.71
5	249.62	273.69	251.06	252.68

TABLE 1. Smallest and largest eigenvalues for the equilateral triangle when $p = 1$ and $p = 50$.

In these two examples, the situation appears to be very different. Thus we recall in the following section some theoretical results regarding properties of the partitions minimizing $\Lambda_{k,\infty}$ as well as criteria allowing to decide whether a partition optimal for the max are not optimal for the sum.

3. Theoretical results

In this section, let us recall some theoretical results about the p-minimal k-partitions. With these theoretical results we can comment on the implementation done in the previous

section. This is also useful to propose some new adaption of the algorithm in the next section.

3.1. **Monotonicity.** First of all, let us recall a monotonicity result.

Theorem 3.1. *Let $k \geq 1$ and $1 \leq p \leq q < \infty$. We have monotonicity*

- *with respect to the domain*
$$\Omega \subset \tilde{\Omega} \quad \Rightarrow \quad \mathfrak{L}_{k,p}(\tilde{\Omega}) \leq \mathfrak{L}_{k,p}(\Omega);$$
- *with respect to the number k of domains of the partition*
$$\mathfrak{L}_{k,p}(\Omega) < \mathfrak{L}_{k+1,p}(\Omega);$$
- *with respect to the p-norm*
$$\frac{1}{k^{1/p}}\mathfrak{L}_{k,\infty}(\Omega) \leq \mathfrak{L}_{k,p}(\Omega) \leq \mathfrak{L}_{k,q}(\Omega) \leq \mathfrak{L}_{k,\infty}(\Omega), \qquad \forall 1 \leq p \leq q < \infty. \tag{3.1}$$

The proof of the third point is based on the monotonicity for the p-norm. Indeed, for any partition $\mathcal{D} \in \mathfrak{P}_k(\Omega)$ and for any $1 \leq p \leq q < \infty$, we have

$$\frac{1}{k^{1/p}}\Lambda_{k,\infty}(\mathcal{D}) \leq \Lambda_{k,p}(\mathcal{D}) \leq \Lambda_{k,p}(\mathcal{D}) \leq \Lambda_{k,\infty}(\mathcal{D}). \tag{3.2}$$

We notice that the results of Table 1 are coherent with (3.1) since $\Lambda_{k,p}(\mathcal{D}^{k,p})$ should be close to $\mathfrak{L}_{k,p}(\triangle)$ and we observe that $\Lambda_{k,1}(\mathcal{D}^{k,1}) \leq \Lambda_{k,50}(\mathcal{D}^{k,50})$.

3.2. **Equipartition.** We say that $\mathcal{D} = (D_1, \ldots, D_k)$ is an *equipartition* if the first eigenvalue on each subdomain $\lambda_1(D_j)$ are equal. The equipartitions play an important rule in these optimization problems. Indeed, as soon as the p-minimal k-partition is an equipartition, it is minimal for any larger q. Furthermore any ∞-minimal k-partition is an equipartition (see[24, Chap. 10]):

Proposition 3.2.

- *If $\mathcal{D}^* = (D_i)_{1\leq i\leq k}$ is a ∞-minimal k-partition, then $\mathcal{D}^*$ is an equipartition:*
$$\lambda_1(D_i) = \mathfrak{L}_{k,\infty}(\Omega)\,, \qquad \text{for any} \quad 1 \leq i \leq k.$$
- *Let $p \geq 1$ and $\mathcal{D}^*$ a p-minimal k-partition. If $\mathcal{D}^*$ is an equipartition, then*
$$\mathfrak{L}_{k,q}(\Omega) = \mathfrak{L}_{k,p}(\Omega), \qquad \text{for any} \quad q \geq p.$$

Consequently, it is natural to set

$$p_\infty(\Omega, k) = \inf\{p \geq 1, \mathfrak{L}_{k,p}(\Omega) = \mathfrak{L}_{k,\infty}(\Omega)\}. \tag{3.3}$$

Let us apply this result in the case of the disk, see Figure 2. If we can prove that the p-minimal k-partition for the norm $p = 1$ and $2 \leq k \leq 5$, is the equipartition with k angular sectors, then according to Proposition 3.2, this partition is minimal for any $p \geq 1$ and $p_\infty(\bigcirc, k) = 1$. In the case of the equilateral triangle, Table 1 makes us think that the p-minimal k-partition is not an equipartition when $k = 2, 4, 5$ and thus $p_\infty(\triangle, k) \geq 50$ in that case.

3.3. **Nodal partition.** When we are interested in optimization problem on partitions whose functional implies spectral quantities it is quite natural to consider nodal partitions. These partitions give, at least, some upper bounds of the optimal energies. Let us recall the definition of a nodal partition.

Definition 3.3. *Let u be an eigenfunction of the Dirichlet-Laplacian on Ω. The nodal sets of u are the components of*

$$\Omega \setminus N(u) \qquad \text{with} \qquad N(u) = \overline{\{x \in \Omega |\, u(x) = 0\}}.$$

The partition composed by the nodal sets is called nodal partition.

Nevertheless, to be useful, it is important to have informations about the number of components of the nodal partitions. According Courant's theorem, any eigenfunction u associated with $\lambda_k(\Omega)$ has at most k nodal domains. An eigenfunction is said *Courant sharp* if it has exactly k nodal domains. The following result, proved by Helffer-Hoffmann–Ostenhof-Terracini [23] gives some bounds using the eigenvalues of the Dirichlet-Laplacian on the whole domain Ω and explicit the cases when we can determine a ∞-minimal k-partition.

Theorem 3.4. *For $k \geq 1$, $L_k(\Omega)$ denotes the smallest eigenvalue (if any) for which there exists an eigenfunction with k nodal domains. We set $L_k(\Omega) = +\infty$ if there is no eigenfunction with k nodal domains. Then we have*

$$\lambda_k(\Omega) \leq \mathfrak{L}_{k,\infty}(\Omega) \leq L_k(\Omega). \tag{3.4}$$

If $\mathfrak{L}_{k,\infty}(\Omega) = L_k(\Omega)$ or $\mathfrak{L}_{k,\infty}(\Omega) = \lambda_k(\Omega)$, then $\lambda_k(\Omega) = \mathfrak{L}_{k,\infty}(\Omega) = L_k(\Omega)$ and then any Courant sharp eigenfunction associated with $\lambda_k(\Omega)$ produces a ∞-minimal k-partition.

Consequently, if there exists a Courant sharp eigenfunction associated with the k-th eigenvalue, then the ∞-minimal k-partition is nodal. Otherwise the ∞-minimal k-partition is not nodal. Note that we have always $\lambda_2(\Omega) = L_2(\Omega)$ (since the second eigenfunctions has exactly two nodal domains), then any ∞-minimal 2-partition is nodal and

$$\mathfrak{L}_{2,\infty}(\Omega) = \lambda_2(\Omega). \tag{3.5}$$

As soon as $k \geq 3$, it is not so easy and it is then important to determine for which k we have equality $\lambda_k(\Omega) = L_k(\Omega)$. Pleijel [26] established that it is impossible for k large:

Theorem 3.5. *There exists k_0 such that $\lambda_k(\Omega) < L_k(\Omega)$ for $k \geq k_0$.*

Therefore, a ∞-minimal k-partition is never nodal when $k > k_0$. This result proves the existence of such k_0 but is not quantitative. Recently, Bérard-Helffer [3] and van den Berg-Gittins [28] exhibit an explicit bound for k_0.

In some specific geometries, we can determine exactly for which eigenvalue $\lambda_k(\Omega)$, there exists an associated Courant sharp eigenfunction. For such k, we thus exhibit a ∞-minimal k-partition whose energy is $\lambda_k(\Omega)$. The following property gives such result for the disk [23, Proposition 9.2], the square [1], and the equilateral triangle [2] (see also references therein).

Proposition 3.6. *If Ω is a square $\square$, a disk $\bigcirc$ or an equilateral triangle $\triangle$, then*

$$\lambda_k(\Omega) = \mathfrak{L}_{k,\infty}(\Omega) = L_k(\Omega) \qquad \text{if and only if} \qquad k = 1, 2, 4.$$

Thus the ∞-minimal k-partition is nodal if and only if $k = 1, 2, 4$.

Figure 4 gives examples of ∞-minimal k-partitions. Note that since $\lambda_2(\Omega)$ is double the ∞-minimal 2-partition is generally not unique whereas for $k = 4$ we do have uniqueness. We note that for $\Omega = \bigcirc, \triangle$ and $k = 2, 4$, we recover the k-partitions obtained numerically in Figures 2 and 3.

3.4. **Bounds with spectral quantities.**

3.4.1. *Lower bounds.* The lower bounds (3.4) can be generalized when considering the p-norm instead of the ∞-norm and we have (see [23] for $p = \infty$ and [21] for the general case)

$$\left(\frac{1}{k}\sum_{i=1}^{k}\lambda_i(\Omega)^p\right)^{1/p} \leq \mathfrak{L}_{k,p}(\Omega) \leq L_k(\Omega). \tag{3.6}$$

When Ω is a square, a disk or an equilateral triangle, the eigenvalues are explicit (see Table 2 where $j_{m,n}$ is the n-th positive zero of the Bessel function of the first kind J_m) and thus they produce explicit lower and upper bounds. Computing the number of nodal domains of some eigenfunctions give us a upper bound for $L_k(\Omega)$ (see Table 3).

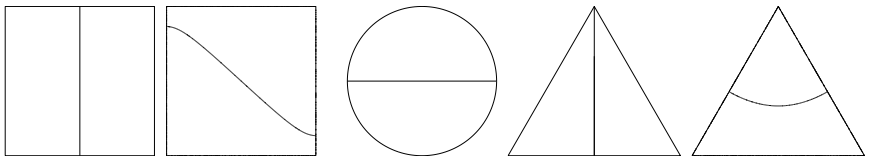

(a) $k = 2$

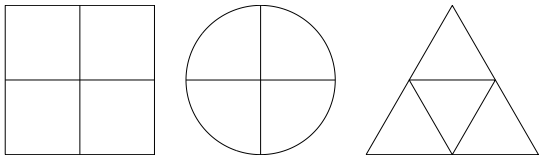

(b) $k = 4$

FIGURE 4. Nodal ∞-minimal k-partitions, $k = 2, 4$

Ω	$\lambda_{m,n}(\Omega)$	m, n
$\square$	$\pi^2(m^2+n^2)$	$m, n \geq 1$
$\triangle$	$\frac{16}{9}\pi^2(m^2+mn+n^2)$	$m, n \geq 1$
$\bigcirc$	$j^2_{m,n}$	$m \geq 0$, $n \geq 1$ (multiplicity 2 for $m \geq 1$)

TABLE 2. Eigenvalues for $\Omega = \square,\ \triangle,\ \bigcirc$.

	Square		Disk		Equilateral triangle	
k	$\lambda_k(\square)$	$\mu(u_k)$	$\lambda_k(\bigcirc)$	$\mu(u_k)$	$\lambda_k(\triangle)$	$\mu(u_k)$
1	19.739	1	5.7831	1	52.638	1
2	49.348	2	14.6819	2	122.822	2
3	49.348	2	14.6819	2	122.822	2
4	78.957	4	26.3746	4	210.552	4
5	98.696	3	26.3746	4	228.098	4
6	98.696	3	30.4713	2	228.098	3
7	128.305	4	40.7065	6	333.373	4
8	128.305	4	40.7065	6	333.373	4
9	167.783	4	49.2184	4	368.465	4
10	167.783	4	49.2184	4	368.465	4

TABLE 3. Lowest eigenvalues $\lambda_k(\Omega)$ and number of nodal sets for associated eigenfunctions u_j of the Dirichlet-Laplacian on $\Omega = \square$, $\bigcirc$ and $\triangle$.

3.4.2. *Upper bounds.* Let us mention that in the case of the disk, we can easily construct a k-partition of $\bigcirc$ by considering the partition with k angular sectors of opening $2\pi/k$. If we denoted by $\Sigma_{2\pi/k}$ an angular sector of opening $2\pi/k$, then we have the upper bound

$$\mathfrak{L}_{k,p}(\bigcirc) \leq \lambda_1(\Sigma_{2\pi/k}). \tag{3.7}$$

Recall that the eigenvalue of a sector Σ_α of opening α are given by (see [9]) :

$$\lambda_{m,n}(\alpha) = j^2_{m\frac{\pi}{\alpha},n},$$

where $j_{m\frac{\pi}{\alpha},n}$ is the n-th positive zero of the Bessel function of the first kind $J_{m\frac{\pi}{\alpha}}$. In particular, we have

$$\lambda_1(\Sigma_{2\pi/k}) = j^2_{\frac{mk}{2},1}.$$

Let us remark that if k is odd, the k-partition with k angular sectors is not nodal and (3.7) gives a new upper bound which can be better than (3.4) or (3.6). If k is even, we have $L_k(\bigcirc) \leq \lambda_1(\Sigma_{2\pi/k})$.

In the case of the square, we will use the following upper bound which is a weaker but more explicit than (3.6):

$$\mathfrak{L}_{k,p}(\square) \leq \inf_{m,n\geq 1}\{\lambda_{m,n}(\square)|mn=k\} \leq \lambda_{k,1}(\square).$$

3.5. **Candidates for the sum and the max.** We have seen in Section 2.4 that the candidates to be minimal for the sum and the max seem to be the same in the case of the disk when $k = 2, 3, 4, 5$ (see Figure 2) whereas they are different for the equilateral triangle when $k = 2, 4, 5$ (see Figure 3). Then it could be interesting to have some criteria to discriminate if a ∞-minimal k-partition can be minimal for the sum ($p = 1$). A necessary condition is given in [22]:

Proposition 3.7. *Let $\mathcal{D} = (D_1, D_2)$ be a ∞-minimal 2-partition and φ_2 be a second eigenfunction of the Dirichlet-Laplacian on Ω having D_1 and D_2 as nodal domains.*

Suppose that $\displaystyle\int_{D_1} |\varphi_2|^2 \neq \int_{D_2} |\varphi_2|^2$, then $\mathfrak{L}_{2,1}(\Omega) < \mathfrak{L}_{2,\infty}(\Omega)$.

Since any ∞-minimal 2-partition is nodal, we can use the previous criterion by considering neighbors in a k-partition.

Proposition 3.8. *Let $\mathcal{D} = (D_i)_{1\leq i\leq k}$ be a k-partition and $D_i \sim D_j$ be a pair of neighbors. We denote $D_{ij} = \mathrm{Int}\overline{D_i \cup D_i}$. There exists a second eigenfunction φ_{ij} of the Dirichlet-Laplacian on D_{ij} having D_i and D_j as nodal domains.*

If $\displaystyle\int_{D_i} |\varphi_{ij}|^2 \neq \int_{D_j} |\varphi_{ij}|^2$, then $\mathfrak{L}_{k,1}(\Omega) < \lambda_2(D_{ij})$.

4. Candidates for the infinity norm

4.1. **Penalization method.** We note that the results obtained in Section 2.4 using the p-norm approach do not consist of exact equipartitions. We recall that this is a necessary condition for a partition to be a solution of the min-max problem (1.3) with $p = \infty$ (see Proposition 3.2). We use the following idea in order to force the eigenvalues to be closer. If we are able to minimize the sum of eigenvalues

$$\lambda_1(D_1) + \ldots + \lambda_1(D_k),$$

under the constraint $\lambda_1(D_1) = \ldots = \lambda_1(D_k)$, we are in fact minimising the maximal eigenvalue. We can, thus, for every parameter $\varepsilon > 0$ consider the smooth functionals

$$F_\varepsilon((D_i)) = \frac{1}{k}\sum_{i=1}^{k} \lambda_1(D_i) + \frac{1}{\varepsilon}\sum_{1\leq i<j\leq k} (\lambda_1(D_i) - \lambda_1(D_j))^2,$$

i.e. the average of the eigenvalues plus a term penalizing pairs of non-equal eigenvalues. If we define the functional

$$F((D_i)) = \begin{cases} \max\{\lambda_1(D_i), 1 \leq i \leq k\} & \text{if } (D_i) \text{ is an equipartition,} \\ +\infty & \text{otherwise,} \end{cases}$$

then we have the following result.

Proposition 4.1. *The functionals F_ε Γ-converge to F, in the sense that*

- *for every $(D_i^\varepsilon) \to (D_i)$ as $\varepsilon \to 0$, $\liminf_{\varepsilon\to 0} F_\varepsilon((D_i^\varepsilon)) \geq F((D_i))$,*
- *for every (D_i), we can find $(D_i^\varepsilon) \to (D_i)$ such that $\limsup_{\varepsilon\to 0} F_\varepsilon((D_i^\varepsilon)) \leq F((D_i))$.*

Consequently any limit point of a sequence of minimizers of F_ε is a minimizer for F.

Proof. Let (D_i^ε) be a sequence of partitions of Ω which converges to (D_i) in the Hausdorff metric. It is clear that (D_i) is also a partition of Ω. Since the Dirichlet-Laplace eigenvalues are stable under the Hausdorff convergence we directly obtain

$$\liminf_{\varepsilon\to 0} F_\varepsilon((D_i^\varepsilon)) \geq F((D_i)).$$

The above inequality is obvious if (D_i) is not an equipartition, since then we have

$$\liminf_{\varepsilon\to 0} F_\varepsilon((D_i^\varepsilon)) = +\infty.$$

On the other hand, if (D_i^ε) is an equipartition we clearly see that the inequality is true since

$$\liminf_{\varepsilon\to 0} F_\varepsilon((D_i^\varepsilon)) \geq \frac{1}{k}\sum_{i=1}^{k} \lambda_1(D_i)) = \max_{1\leq i\leq k} \lambda_1(D_i).$$

The $\Gamma-\limsup$ part is straightforward by choosing a constant sequence. □

We use the result of Proposition 4.1 to construct a numerical algorithm which approaches the min-max problem (1.3) with $p=\infty$. We minimize the functional F_ε for $\varepsilon \in \{10, 1, 0.1, 0.01\}$ and each time we start from the result of the previous optimization. In the minimization of F_ε we use the same discrete framework presented in Section 2.4 as well as the penalized eigenvalue problem (2.2). In Table 4 we present the minimal and maximal eigenvalues obtained when minimizing $\Lambda_{k,50}$ and when using the penalization method described in this section, that is to say

$$\min\{\lambda_1(D_j), 1\leq j\leq k\} \quad \text{and} \quad \max\{\lambda_1(D_j), 1\leq j\leq k\},$$

where (D_j) is either the numerical p-minimal k-partition $\mathcal{D}^{k,p}$ for $p=50$ or the partition obtained with the penalization method. We also added the relative differences between maximal and minimal eigenvalues. Comparing these differences we note that the penalization method gives partitions which are closer to being an equipartition. We also observe that the maximal value among the first eigenvalues is lower for the penalization method. Thus this method gives us better candidates. The partitions obtained with the penalization method are presented in Figure 5.

Ω	k	$\mathfrak{L}_{k,50}(\Omega)$			penalization		
		min	max	diff.(%)	min	max	diff.(%)
△	4	208.92	211.71	1.32	209.15	211.04	0.89
	5	249.17	252.67	1.38	251.27	252.17	0.36
	6	275.37	276.16	0.28	275.34	276.22	0.31
	7	338.04	348.24	2.92	343.51	345.91	0.69
	8	388.47	391.06	0.66	388.46	389.53	0.27
	9	422.80	431.92	2.11	425.34	428.74	0.79
	10	445.50	456.66	2.44	450.74	453.25	0.55
□	5	103.75	105.82	1.95	104.24	104.60	0.34
	6	125.79	128.11	1.81	126.36	128.14	1.38
	7	144.49	147.44	2.00	145.81	146.90	0.74
	8	160.48	161.64	0.71	160.76	161.28	0.32
	9	176.64	179.21	1.49	177.13	178.08	0.53
	10	200.00	206.85	3.31	202.78	204.54	0.86

TABLE 4. Minimal and maximal eigenvalues of the candidates obtained by the p-norm and the penalization methods.

Since in the cases $k=2,4$ we know the explicit optimizers we summarize in Table 5 the results obtained with our numerical approaches in these two cases. We observe that the penalization method produces better candidates.

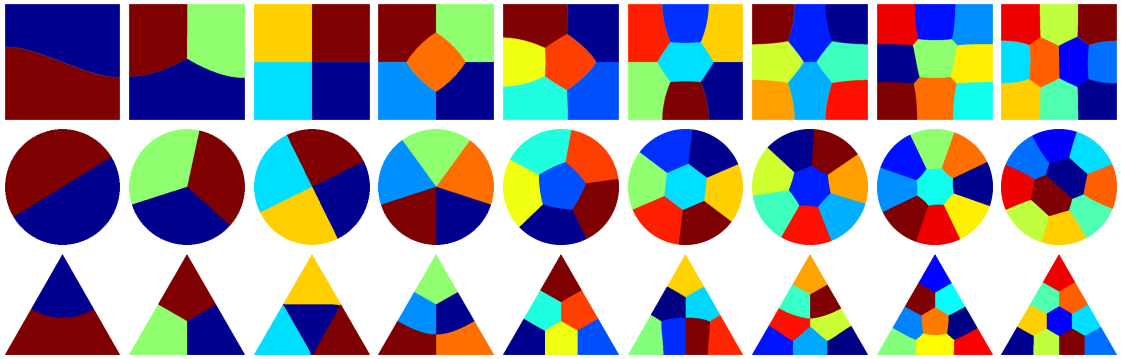

FIGURE 5. Partitions obtained with the penalization method.

	Disk			Square			Equilateral triangle		
k	$p=50$	pen.	explicit	$p=50$	pen.	explicit	$p=50$	pen.	explicit
2	20.25	20.24	20.19	49.348	49.348	49.348	123.38	122.96	122.82
4	26.42	26.42	26.37	78.957	78.957	78.957	211.71	211.04	210.55

TABLE 5. Comparison of the two methods for $\Omega = \bigcirc, \square, \triangle$ in explicit cases.

Synthesized results are presented in Table 6 where we also present the values obtained with the mixed Dirichlet-Neumann method presented in the next section.

4.2. **Dirichlet-Neumann approach.** The penalization method proposed in the previous section gives improved results in some situations as compared to the p-norm method. Still, the results we obtain are close, but not precisely an equipartition, as the theoretical results state in Proposition 3.2 presented in the previous section. In this section we propose a method which in some cases allows us to search precisely for an equipartition. In this approach, we try to find symmetric candidates whose energy is lower than the ones obtained before. Nevertheless, we use the previous methods in order to have an idea of the structure of the optimal partition and thus look now for partitions where we have fixed some parts of the boundaries of the subdomains. Note that for $k = 2$ any minimal 2-partition for $\mathfrak{L}_{2,\infty}$ is a nodal partition for the second eigenvalue of the Dirichlet-Laplacian on Ω (see Theorem 3.4 and (3.5)). According to Proposition 3.6, when $\Omega = \square$, $\bigcirc$, $\triangle$, no ∞-minimal k-partition is nodal except for $k = 1, 2, 4$. This is also observed numerically because the partitions we exhibit for $k \notin \{2, 4\}$ have critical points with degree at least three.

The idea is to search for minimal partitions with the aid of nodal sets of a certain mixed Dirichlet-Neumann problem. This approach has already been used in [8] for the study of the 3-partitions of the square and the disk. In the following we identify other situations where the method applies. In those cases the partition obtained with the Dirichlet-Neumann method is an exact equipartition and it allows us to decrease even more the value of $\Lambda_{k,\infty}$ (see Table 6).

Let us take the case of the 3-partition in the equilateral triangle as an example. The notations are presented in Figure 6. Figure 6(a) gives the partition obtained by one of the iterative methods. We represent below the partition with the symmetry axis AD and the triple point D_r. It is not difficult to see that this partition can be regarded as a nodal partition if we consider a mixed Dirichlet-Neumann problem with the Dirichlet condition on the segment $[\mathsf{DD}_r]$ and the Neumann condition on the segment $[\mathsf{AD}_r]$. We also note that the additional symmetry of the partition allows us to work only on the triangle ABD. Thus, the working configuration is the triangle ABD with Dirichlet boundary conditions on $[\mathsf{DD}_r], [\mathsf{DB}]$ and $[\mathsf{AB}]$ and a Neumann boundary condition on $[\mathsf{AD}_r]$. We take the point D_r variable on $[\mathsf{AD}]$ and we look for the position of D_r for which the nodal line touches the

segment $[\mathsf{DD}_r]$ and for which the value of the second eigenvalue is minimal. Figures 6(b) give examples of nodal partitions according to the position of the mixed Dirichlet-Neumann point. In the following we make the convention that red lines signify Dirichlet boundary conditions and blue dotted lines represent Neumann boundary conditions.

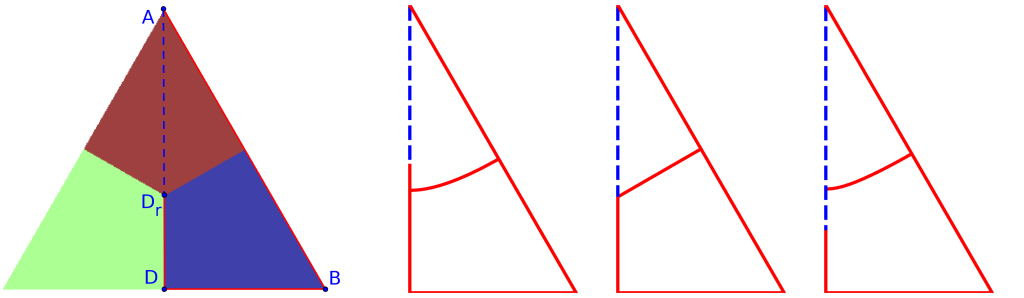

(a) $\mathcal{D}^{3,50}$ (b) Nodal lines according to the position of the mixed point

FIGURE 6. Dirichlet-Neumann approach for 3-partitions of the equilateral triangle.

The square. We start with the case of 3-partitions and we recall the results obtained in [8]. The iterative algorithm gives a partition with an axis of symmetry parallel to the sides. Therefore we choose to impose a mixed condition on this axis, working on only half the square. Figure 7 illustrates the choice of the mixed problem and the results. We obtain numerically that the triple point is at the center and that the value of the second Dirichlet-Neumann eigenvalue on the half-domain is 66.5812. As it was noted in [8], choosing a mixed condition on the diagonal instead gives another partition with the same energy. Moreover, in [7], it is shown that we have a continuous family of partitions with the same energy.

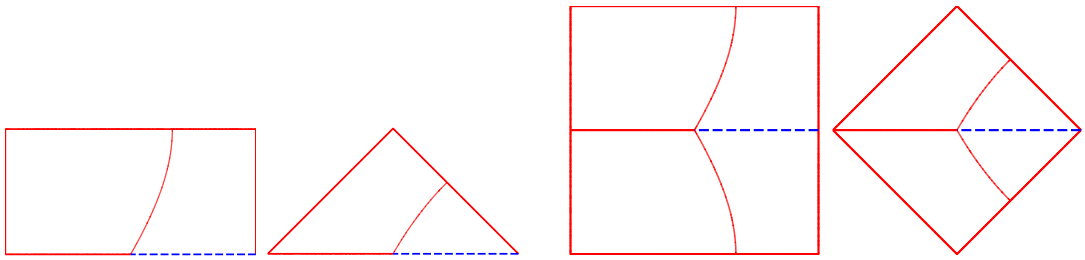

(a) Two mixed Dirichlet-Neumann configurations (b) Candidates for the ∞-minimal 3-partition

FIGURE 7. Dirichlet-Neumann approach for 3-partitions of the square.

In the case of the 5-partition of the square we note that the partition obtained by the iterative algorithm seems to have the same axes of symmetry as the square. Due to the symmetry of the partition one can consider a mixed Dirichlet-Neumann problem on an eighth of the square as seen in Figure 8(a). The second Dirichlet-Neumann eigenfunction of this configuration has nodal domains which extend by symmetry to a 5-partition of the square. The second eigenvalue of this mixed configuration is equal to the first Dirichlet eigenvalue on each cell of the 5-partition built after symmetrization (see Figrue 8(b). This second Dirichlet-Neumann eigenvalue, equal to 104.294, gives a upper bound for $\mathfrak{L}_{5,\infty}(\square)$ which is lower than the ones obtained with the iterative methods.

The Disk. We know that the ∞-minimal k-partition consists in k equal sectors when $k = 2, 4$. Numerically, it seems to be the same for $k \in \{3, 5\}$ and some works tried to prove it when $k = 3$ (see [21, 6]).

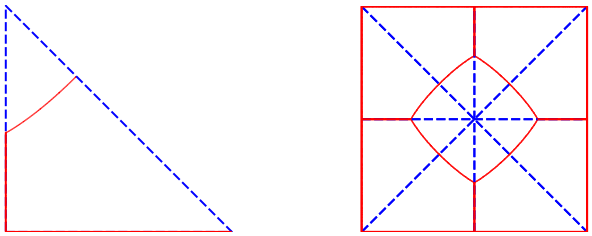

(a) Mixed problem (b) Symmetriezd 5-partition

FIGURE 8. Dirichlet-Neumann approach for 5-partitions of the square.

For larger k ($k \in [6,9]$), we observe that numerical partitions obtained with the iterative method consist of a structure which is invariant by a rotation of $2\pi/(k-1)$. This motivates us to use the Dirichlet-Neumann approach for the cases $k \in [6,9]$. Indeed, one can see that the invariance by a rotation of angle $2\pi/(k-1)$ allows us to represent exterior cells of the configurations as subsets of a sector of angle $2\pi/(k-1)$. This brings us to consider a mixed Dirichlet-Neumann problem on such sectors. If we consider the center of the disk at the origin, and we denote the sector by $\widehat{\mathsf{OAB}}$ then for $r \in (0,1)$ we consider the points $\mathsf{A}_r \in [\mathsf{OA}]$ and $\mathsf{B}_r \in [\mathsf{OB}]$ with $\mathsf{A}_r\mathsf{O} = \mathsf{B}_r\mathsf{O} = r$. We consider Neumann boundary conditions on $[\mathsf{O},\mathsf{A}_r]$, $[\mathsf{O},\mathsf{B}_r]$ and Dirichlet condition on $[\mathsf{A}_r\mathsf{A}]$, $[\mathsf{B}_r\mathsf{B}]$ and the arc AB. Figure 9 illustrates this mixed Dirichlet-Neumann configuration. Next we vary r in $(0,1)$ and we record the

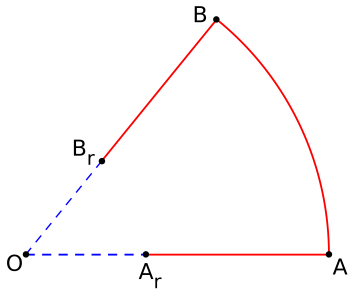

FIGURE 9. The setup for the mixed problem on sectors.

position where the nodal line associated to the second eigenfunction of the Laplace operator with these mixed boundary conditions touches the segments $[\mathsf{A}_r\mathsf{A}]$, $[\mathsf{B}_r\mathsf{B}]$. This is necessary in order to have a k-partition after symmetrization. On the other hand we want the largest possible r in order to obtain minimal eigenvalues in the symmetrized partition of the disk (since the eigenvalue of the mixed problem is decreasing when r is increasing). Thus, for each $k \in [6,9]$ we consider the above mixed problem in the sector of angle $2\pi/(k-1)$ and we search in each case for the optimal value of r. The second eigenvalue of the mixed problem equals the first eigenvalue of each domain of the partition obtained by the symmetrization of this eigenvalue to the whole disk. The values obtained are recorded in Table 6 and the partitions are given in Figure 10. We note that for $k = 10$ the same approach in a sector of angle $2\pi/9$ gives a candidate which has a larger energy than the partition obtained with the iterative algorithm.

Equilateral triangle. In this case we also have some configurations where we can apply the Dirichlet-Neumann method. In the cases $k = 3, 6, 10$ the partitions obtained by the iterative algorithm have the three axes of symmetry of the equilateral triangle. This allows us to reduce the problem to the study of mixed problems on a half or a sixth of the equilateral triangle. We also observe a possible application of the method to the case $k = 5$ where we may consider Dirichlet boundary condition on part of the height of the triangle.

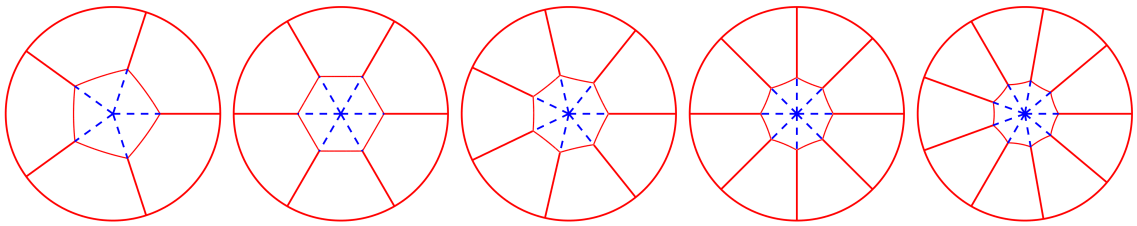

FIGURE 10. Candidates for the ∞-minimal k-partitions on the disk with the Dirichlet-Neumann approach, $6 \leq k \leq 10$.

The case $k = 8$ also lets us use a mixed problem with Dirichlet boundary condition on part of the height and a vertical mobile segment.

We start with $k = 3$ where the optimal candidate seems to be made of three congruent quadrilaterals with a common vertex at the centroid and each one having a pair of sides orthogonal to the sides of the triangle. Note that a brief idea of the method was described in Figure 6. We consider a mixed Dirichlet Neumann problem on half of the equilateral triangle. Let ABD be half of the equilateral triangle, where AD is one of the heights of the triangle (see Figure 11). We consider a mobile point D_r on the segment $[\mathsf{AD}]$ and we compute the second eigenvalue of the Dirichlet Laplace operator with Dirichlet boundary conditions on segments $[\mathsf{D}_r\mathsf{D}], [\mathsf{DB}], [\mathsf{AB}]$ and Neumann conditions on $[\mathsf{AD}_r]$. The choice of the Dirichlet boundary condition on $[\mathsf{D}_r\mathsf{D}]$ was motivated by the structure of the result in the iterative algorithm. We may ask what happens when we interchange the boundary condition on the height $[\mathsf{AD}]$, *i.e.* considering Dirichlet boundary condition on $[\mathsf{AD}_r]$ and Neumann boundary condition on $[\mathsf{D}_r\mathsf{D}]$. This is discussed at the end of this section in Remark 4.2. Next we vary the position of D_r on $[\mathsf{AD}]$ so that the nodal line of the second eigenvalue of the mixed problem touches $[\mathsf{DD}_r]$ exactly at D_r. As expected the position where we obtain this configuration is for $\mathsf{DD}_r = \mathsf{AD}/3$ which means that the triple point of the symmetrized partition is the centroid of the equilateral triangle.

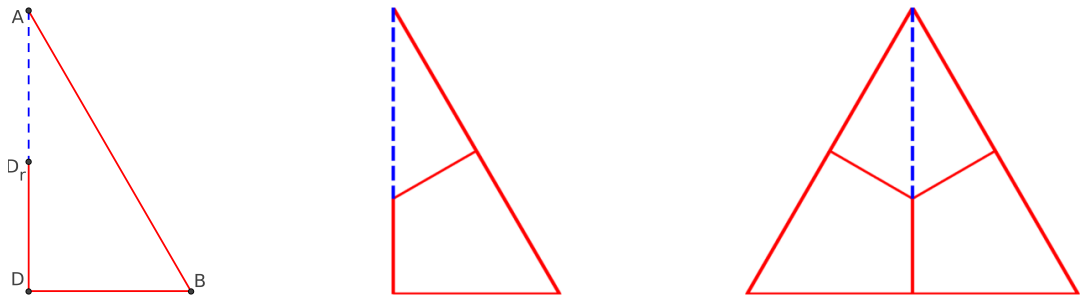

(a) Mixed problem (b) Optimal nodal partition (c) Symmetrized partition

FIGURE 11. Dirichlet-Neumann approach for 3-partitions of the equilateral triangle.

The case $k = 5$ can be treated in the same framework, but instead of looking at the second eigenfunction of the mixed problem we study the third one. The result is presented in Figure 12. In optimal configuration, the triple point is such that $\mathsf{DD}_r = \mathsf{AD}/2$.

We continue with the case $k = 8$ where we can also use a Dirichlet Neumann approach on half of the equilateral triangle. Here we observe that in addition to the axis of symmetry, one of the common boundaries between the cells also seems to be a vertical segment. We use this fact to define a mixed eigenvalue problem with four parameters on half of the equilateral triangle. Like in Figure 13 we consider four variable points defined as follows. We consider the triangle ABD where AD is a height of the equilateral triangle. On the side AD we consider two variable points $\mathsf{X}_s, \mathsf{X}_t$. On the segment $[\mathsf{X}_s, \mathsf{X}_t]$ we put a Dirichlet boundary condition and on the segments $[\mathsf{AX}_s], [\mathsf{DX}_t]$ we have Neumann boundary conditions. We

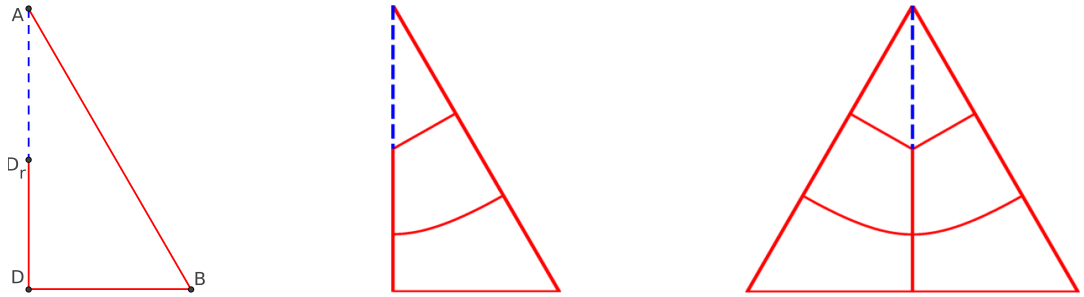

(a) Mixed problem (b) Optimal nodal partition (c) Symmetrized partition

FIGURE 12. Dirichlet-Neumann approach for 5-partitions of the equilateral triangle.

consider another variable point $\mathsf{Y}_r \in [\mathsf{BD}]$ and we construct Y_q such that $\mathsf{Y}_q\mathsf{Y}_r \perp \mathsf{BD}$ with the length of $[\mathsf{Y}_r\mathsf{Y}_q]$ as a variable. On the segment $[\mathsf{Y}_q\mathsf{Y}_r]$ we put a Dirichlet boundary condition. Of course, the remaining segments $[\mathsf{AB}], [\mathsf{BD}]$ also have a Dirichlet boundary conditions. We vary the position of these four points so that the fifth eigenfunction of the mixed problem has nodal lines which touch the Dirichlet parts at their extremities. The choice of the fifth eigenvalue is motivated by the fact that we need a nodal 5-partition so that the symmetrized partition would have 8 cells. The optimal configuration is shown in Figure 13.

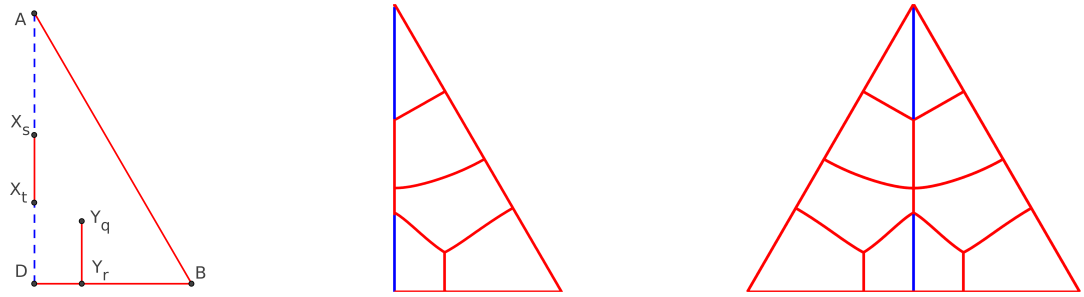

(a) Mixed problem (b) Optimal nodal partition (c) Symmetrized partition

FIGURE 13. Dirichlet-Neumann approach for 8-partitions of the equilateral triangle

In the case $k = 6$ the optimal partition obtained with the iterative algorithm has three axes of symmetry. Using this we can reduce the problem to the study of a mixed problem on one sixth of the equilateral triangle, *i.e.* a subtriangle defined by a vertex, the feet of a height and the centroid of the triangle. As in Figure 14(a) we consider the triangle defined by a vertex A, the feet of an altitude D and the centroid C. On the side AC we consider a mobile point $\mathsf{X}_r = r\mathsf{A} + (1-r)\mathsf{C}$ for $r \in (0,1)$. We note that the candidate obtained with the iterative algorithm seems to correspond to a mixed problem on the triangle ACD with Dirichlet boundary conditions on segments $[\mathsf{AD}]$ and $[\mathsf{CX}_r]$ and Neumann boundary conditions on $[\mathsf{CD}]$ and $[\mathsf{AX}_r]$. We search for the position of X_r such that the nodal line of the second eigenfunction touches the segment $[\mathsf{CX}_r]$ precisely at X_r (see Figure 14(b)). The optimal nodal configuration and the partition obtained by performing symmetrizations is represented in Figure 14(c).

In the case $k = 10$ we observe that the partition has again three axes of symmetry and we may try to represent it as a mixed Dirichlet-Neumann problem on a sixth of the equilateral triangle. Consider the same starting triangle ACD like for $k = 6$. Pick the variable points $X_r = (1-r)A + rD$ on $[AD]$ and $X_s = sC + (1-s)D$. Construct $Y_r \in [AC]$ such that $\mathsf{X}_r\mathsf{Y}_r \perp \mathsf{AD}$ and $\mathsf{Y}_s \in [\mathsf{AC}]$ such that $\widehat{\mathsf{X}_s\mathsf{C}\mathsf{Y}_s} = \pi/3$ (to satisfy the equal angle

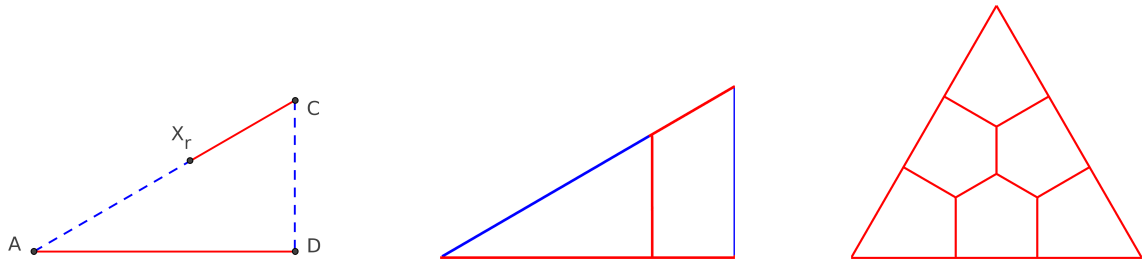

(a) Mixed problem (b) Optimal nodal partition (c) Symmetrized partition

FIGURE 14. Dirichlet-Neumann approach for 6-partitions of the equilateral triangle.

property). If we pick the origin at A and D of coordinates $(0.5, 0)$ then we obtain the following coordinates for all the above defined points: $\mathsf{C}(0.5, \sqrt{3}/6)$, $\mathsf{X}_r(r, 0)$, $\mathsf{Y}_r(r, r\sqrt{3}/3)$, $\mathsf{X}_s(0.5, s\sqrt{3}/6)$, $\mathsf{Y}_s(0.25 + s\sqrt{3}/2, \sqrt{3}/12 + s/2)$. As in the Figure 15(a) we take a Dirichlet boundary condition on segments $[\mathsf{AD}], [\mathsf{DX}_s], [\mathsf{Y}_s\mathsf{Y}_r]$ and Neumann boundary condition on segments $[\mathsf{AY}_r], [\mathsf{CY}_s], [\mathsf{CX}_s]$. Since the numerical candidate in this case seems to have cells with polygonal borders we search the positions of X_r and X_s such that the nodal lines of the third eigenfunctions of the eigenvalue problem with mixed boundary conditions are exactly the segments $[\mathsf{X}_r\mathsf{Y}_r]$ and $[\mathsf{X}_s\mathsf{Y}_s]$. The result is shown in Figure 15 together with the symmetrized partition.

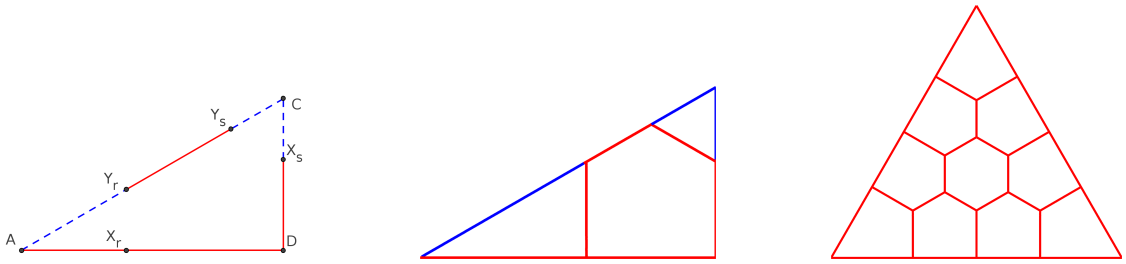

(a) Optimal nodal partition (b) Optimal nodal partition (c) Symmetrized partition

FIGURE 15. Dirichlet-Neumann approach for 10-partitions of the equilateral triangle.

Remark 4.2. In some cases we have chosen the Dirichlet and Neumann parts of the mixed problem based on the results given by the iterative method. We may ask what happens if we permute the two conditions.

For the case $k = 3$ on the equilateral triangle, if we consider Dirichlet boundary condition on segment $[AD_r]$ and Neumann boundary condition on $[\mathsf{DD}_r]$ (see Figure 11(a) for the notations) then the optimal configuration is again when $DD_r = AD/3$, but the eigenvalues of the cells on the symmetrized domain are strictly higher than the one obtained before.

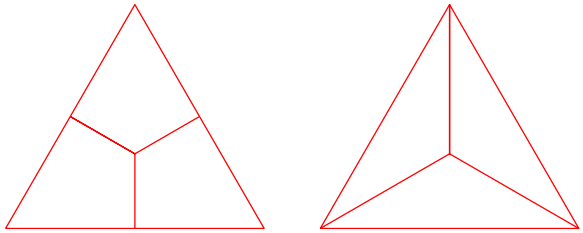

$\Lambda_{3,\infty} = 142.89$ $\Lambda_{3,\infty} = 215.13$

FIGURE 16. Dirichlet-Neumann approach for 3-partitions of the equilateral triangle.

For the case $k = 5$ on the square we have seen that the partition seems to have all the symmetry axes of the square. As suggested by the result of the iterative method we considered a Dirichlet-Neumann condition corresponding to an axis of symmetry parallel to the sides of the square. As shown in [5, Figure 19] choosing a mixed boundary condition on the diagonal gives a partition with a strictly higher maximal eigenvalue.

Remark 4.3. We note the similarity of the partitions of the equilateral triangle for $k = 3$ and $k = 5$ to some eigenvalues of the Aharonov-Bohm operator on a sector considered in [9, 11]. Thus we were able to check that the partition for $k = 3$ corresponds to the third eigenvalue of the Aharonov-Bohm operator on the equilateral triangle with a singularity at its centroid. In the same way, the partition for $k = 5$ corresponds to the sixth eigenvalue of the Aharonov-Bohm operator on the equilateral triangle with a singularity at the midpoint of one of the heights.

4.3. **Summary of the numerical results.** We have seen three numerical approaches for the study of the minimizers of $\mathfrak{L}_{k,\infty}$: the use of p-norms of eigenvalues with p large, the penalization method and the Dirichlet-Neumann method. We make below a brief analysis and a comparison of the results given by these methods.

First we note that the p-norms method and the penalization method work in all cases. In most of the cases, the penalization method does exactly what it was build for: penalize the difference between the eigenvalues while minimizing their sum. Thus there is no great surprise to see that it manages to give better upper bounds for $\mathfrak{L}_{k,\infty}(\Omega)$. As we can see in Table 4 the penalization method produces results where the gap between the minimal and maximal eigenvalues of cells is smaller. Inspiring from the results of the iterative methods, we can improve them by restricting the research to some particular partitions where we fixe some parts of the boundaries of the subdomains: this is the Dirichlet-Neumann approach. Once the structure is fixed, we express the partition as a nodal set of a mixed problem. In this paper, we apply this method only with fixed straight lines and symmetry. On the other hand, when the Dirichlet-Neumann can be applied, it produces equipartitions and thus gives the best upper bounds for $\mathfrak{L}_{k,\infty}(\Omega)$. Table 6 summarize the lowest energy $\Lambda_{k,\infty}(\mathcal{D})$ obtained according to the three methods (iterative method for $p = 50$, penalization and Dirichlet-Neumann approach), and thus we deduce some upper bounds for $\mathfrak{L}_{k,p}(\Omega)$.

	Disk			Square			Equilateral triangle		
k	$p = 50$	pen.	D-N	$p = 50$	pen.	D-N	$p = 50$	pen.	D-N
3	20.25	20.24	20.19	66.69	66.612	66.581	143.06	142.88	142.88
5	33.31	33.31	33.21	105.82	104.60	104.29	252.67	252.17	251.99
6	39.40	39.17	39.02	128.11	127.11	-	276.16	276.22	275.97
7	44.26	44.25	44.03	147.44	146.88	-	348.24	345.91	-
8	50.46	50.64	50.46	161.64	161.28	-	391.06	389.53	389.31
9	58.28	58.30	58.25	179.21	178.08	-	431.92	428.75	-
10	64.54	64.27	67.19	206.85	204.54	-	456.66	453.25	451.93

TABLE 6. Lowest energies $\Lambda_{k,\infty}$ for the three methods, $\Omega = \bigcirc,\ \square,\ \triangle$.

The Disk. We notice that for $k \in [2, 5]$ the optimal partitions correspond to sectors of angle $2\pi/k$ and we use the upper bound (3.7) to fill the third column for the disk in Table 6.

For $k \in [6, 9]$ the best candidates are given by the Dirichlet-Neumann approach on sectors of opening $2\pi/(k-1)$; the other two methods give close but larger results.

When $k = 10$, we can also apply a Dirichlet-Neumann approach on an angular sector of opening $2\pi/9$ but the upper bound is worse than with the iterative methods. Indeed, we observe that the optimal 10-partition seems to have two subdomains at the center (see Figure 5).

The Square. For $k \in \{3, 5\}$, it is possible to use the Dirichlet-Neumann method and this gives the lowest upper bound for $\mathfrak{L}_{k,\infty}(\square)$. As shown in [5, Figure 8] for $k = 3$ we have a continuous family of solutions, each with the same maximal eigenvalue.

In other cases, the penalization method gives the best upper bounds for $\mathfrak{L}_{k,\infty}(\square)$. Let us note that for $k = 9$ we are not able to obtain partitions which have a lower maximal eigenvalue than the partition into 9 equal squares, for which all cells have eigenvalue 177.65. On the other hand, since the partition into 9 squares is nodal and the 9-th eigenfunction on the square is not Courant sharp, this is not a ∞-minimal 9-partition (see Theorem 3.4). In our computations, with the p-norm and penalization approaches we find partitions whose energy $\Lambda_{k,\infty}$ equals 179.21 and 178.08 respectively. Since our computations using iterative methods were based on a relaxed formulation for the eigenvalues, the limited numerical precision of the method does not enable us to reach better results whereas we know that the minimal 9-partition has an energy less than 177.65.

The Equilateral triangle. The equilateral triangle gives us lots of occasions where a Dirichlet-Neumann method can be used. For $k \in \{3, 5, 6, 8, 10\}$ this method gives us the best known upper bound for $\mathfrak{L}_{k,\infty}(\triangle)$. For the cases $k \in \{7, 9\}$ the penalization method gives lowest upper bounds. When $k \in \{3, 6, 10\}$ numerical simulations produce partitions hose subdomains are particular polygons with straight lines and it seems this behavior appears for some specific values of k.

Remark 4.4. (Remark about partitions corresponding to triangular numbers) We note that in cases where k is a triangular number, i.e. $k = n(n+1)/2$ with $n \geq 2$, the p-minimal k-partition of the equilateral triangle seems to be the same for any p and to be made of three types of polygonal cells: 3 quadrilaterals at corners which are each a third of an equilateral triangle, $3(n-2)$ pentagons with two right angles and three angles measuring $2\pi/3$ and a family of regular hexagons. In Figure 17 we represent some of the results obtained numerically with the iterative method for $k \in \{15, 21, 28, 36\}$.

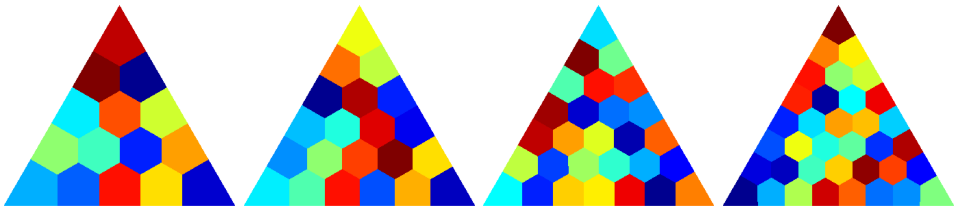

FIGURE 17. Numerical candidates for $k \in \{15, 21, 28, 36\}$.

4.4. **Candidates for the max** *vs.* **the sum.** Given a candidate for minimizing $\Lambda_{k,\infty}$ we may wonder if this partition can also minimize the sum of the eigenvalues $\Lambda_{k,1}$. Such a discussion has already been made in [22] for $k = 2$ and it is concluded that, in general, we have $\mathfrak{L}_{2,1}(\Omega) < \mathfrak{L}_{2,\infty}(\Omega)$. A criterion which allows us to make a decision in some cases was given in Proposition 3.8. Since the optimal partition for $\Lambda_{k,\infty}$ is an equipartition, given two neighbors D_i and D_j from this partition, we have that (D_i, D_j) forms a nodal partition for $\mathrm{Int}\,\overline{D_i \cup D_j}$. Our interest is to see whether the eigenfunction associated to this nodal partition has the same L^2 norm on the two domains D_i, D_j. In the case when the L^2 norms are different we conclude that, supposing the initial partition was optimal for the max, the corresponding partition is not optimal for the sum. Since the criterion can only be applied to equipartitions we quickly examine the candidates obtained with the Dirichlet-Neumann approach.

Let's first remark that Proposition 3.8 does not allow us to say anything about the cases where the optimal partition for the max is made out of congruent elements. In this case the L^2 norms on the subdomains will evidently be the same. This is the case for the $k \in \{2, 4\}$ on the square, $k \in \{3, 4\}$ on the equilateral triangle and $k \in \{2, 3, 4, 5\}$ on the disk.

For the other situations, let us apply Proposition 3.8 at the results obtained with the Dirichlet-Neumann method. For the cases $k \in \{5, 7, 8, 9\}$ for the disk, $k \in \{3, 5\}$ for the square and $k \in \{5, 8\}$ for the equilateral triangle we always find two adjacent domains D_i, D_j in the partition for which the second eigenfunction on $D_i \cup D_j$ has different L^2 norms on D_i, D_j (with a gap larger than 0.03 for normalized eigenfunction). We can conclude that if the above configurations are optimal for the max then they are not optimal for the sum.

Let us analyze below in more detail the situation where Proposition 3.8 does not allow us to conclude. For the equilateral triangle with $k = 6$ or $k = 10$, the gap when we apply the L^2 norm criterion is less than 10^{-4}. In these situations, the subdomains of the numerical ∞-minimal k-partition seem to be polygons with straight lines: quadrilateral, pentagon and regular hexagon (for $k = 10$). If we consider only partitions whose subdomains are like this, we will now compare the best partitions for the sum or the max. Let us discuss a little more these two situations $k = 6$ and $k = 10$ below.

- $k = 6$: the partition is represented in Figure 14. We perform a one parameter study with respect to $r \in [0, 1]$ just as in the case of the Dirichlet-Neumann approach where we compute numerically the eigenvalues on the two types of polygonal cells present in the partition (quadrilateral and pentagon). Numerically we find that the partitions minimizing the max and the sum are almost the same, in the sense that the difference between the values of r which minimize the sum and the max is smaller than 10^{-4}. Thus, the partitions minimizing the sum and the max are either the same or are too close to be distinguished numerically.
- $k = 10$: the partition is represented in Figure 15. We can see that we have three types of domains: a regular hexagon in the center, six pentagons and three quadrilaterals. As in the Dirichlet-Neumann mixed approach, we note that we can characterize the partition using two parameters $t, s \in [0, 1]$. Next we search for the parameters which optimize the maximal eigenvalue and the sum. To obtain an equipartition (for the max), we need to consider non symmetric pentagon. As for $k = 6$, it seems that the optimal partitions are the same for the sum and the max (or very close). The difference between corresponding parameters is again smaller than 10^{-4}.

This suggests that

$$p_\infty(\triangle, k) = 1, \qquad \text{for } k = 6,\ 10.$$

Next is the case of the disk for $k = 7$. Here we also have L^2 norms which are close (the gap is around 0.03) and we analyze this case more carefully in the following sense. Note that the central domain seems to be a regular hexagon $\hexagon$ and the exterior domains D_i $(i = 1, \dots, 6)$ are subsets of angular sector of opening $\pi/3$. We optimize the sum and the max by varying the size of the interior hexagon. Using two different finite element methods, Mélina and FreeFem++, we obtain that the sum is minimized when the side of the hexagon is equal to 0.401 and the maximum is minimized for a side equal to 0.403. These computations let us think that the optimal partitions for the sum and the max might be different in this case. In the following Table 7, we give the parameters for which the sum $\Lambda_{7,1}$ and the maximal eigenvalue $\Lambda_{7,\infty}$ are minimized, as well as the corresponding eigenvalues. We observe that $\Lambda_{7,1}(\mathcal{D}^{7,1}) < \Lambda_{7,\infty}(\mathcal{D}^{7,\infty})$ in coherence with (3.1) and that the gap between the eigenvalues of the minimizer for the sum is significant enough to say that this partition is not an equipartition. Consequently, if the minimal 7-partition of the disk for the max has the previous structure (a regular hexagon at the center and straight lines to join the boundary), it seems that this partition is not minimal for the sum.

In the following section a more detailed analysis is devoted to showing the difference between the partitions minimizing the sum and the ones minimizing the maximal eigenvalue by looking at the evolutions of the partitions with respect to p when minimizing the p-norm of eigenvalues.

r	$\lambda_1(\bigcirc)$	$\lambda_1(D_1)$	$\Lambda_{7,\infty}$	$\Lambda_{7,1}$
0.401	44.498	43.949	44.498	44.028
0.403	44.030	44.030	44.030	44.030

TABLE 7. Upper bounds for $\mathfrak{L}_{7,p}(\bigcirc)$ for $p = 1$ and $p = \infty$.

5. Numerical results for the p-norm

5.1. **Overview.** Our main interest when studying numerically the optimizers of the p-norm of the eigenvalues was the approximation of the $\mathfrak{L}_{k,\infty}$ problem. As we have seen before, the numerical p-minimal k-partition for $p = 50$ is not far from being an equipartition. In this section we make some remarks, based on the numerical simulations, concerning the behavior of the p-minimal k-partitions with respect to p. We are interested in observing the evolution of the configuration of the partitions as p varies from 1 to 50. In most cases the configuration is stable, but there are, however, some cases where the partitions change as p grows and converge to different topological configurations when p goes to ∞. Viewing the evolution of the maximal eigenvalue and the p-norm as p grows can also confirm the conclusions of the previous section concerning the fact that some partitions which optimize the maximal eigenvalue may not optimize the sum. In the following, we will consider the three geometries $\Omega = \triangle, \square, \bigcirc$ and some values of k.

For each of these parameters two figures will highlight the evolution of the p-minimal k-partitions $\mathcal{D}^{k,p}$ obtained by the iterative method. The first one concerns the evolution of the energies: we represent $p \mapsto \Lambda_{k,p}(\mathcal{D}^{k,p})$ in blue, $p \mapsto \Lambda_{k,\infty}(\mathcal{D}^{k,p})$ in red and eventually the upper bound $L_k(\Omega)$ or $\Lambda_k^{DN}(\Omega)$ obtained by the Dirichlet-Neumann approach in magenta (see Figures 18(a), 19(a), 22(a), 23(a), 25(a), 27, 28). In these graphes, we observe that the curve $p \mapsto \Lambda_{k,p}(\mathcal{D}^{k,p})$ (in blue) is increasing, in coherence with (3.1). The decay of the curves $p \mapsto \Lambda_{k,\infty}(\mathcal{D}^{k,p})$ (in red) show that as p is increasing, we get a better and better upper-bound for $\mathfrak{L}_{k,\infty}(\Omega)$. Theses two curves converge to the same value, which is the upper bound obtained by the Dirichlet-Neumann approach when it can be applied. We also illustrate the evolution of the boundary of $\mathcal{D}^{k,p}$ according to p with $p = 1$ in blue and $p = 50$ in red (see Figures 18(b), 19(b), 20, 22(b), 23(b), 24, 25, 26(b)-26(c), 27, 28).

5.2. **The equilateral triangle.** The equilateral triangle is a first example where the optimal partitions for $p = 1$ and $p = \infty$ do not coincide, as seen in the previous section (see also [22] for $k = 2$). Figure 18 represents the evolution of the energies and the optimal partitions as p increases. We observe that even if the partitions do not change much, the maximal eigenvalue is significantly decreased as p increases.

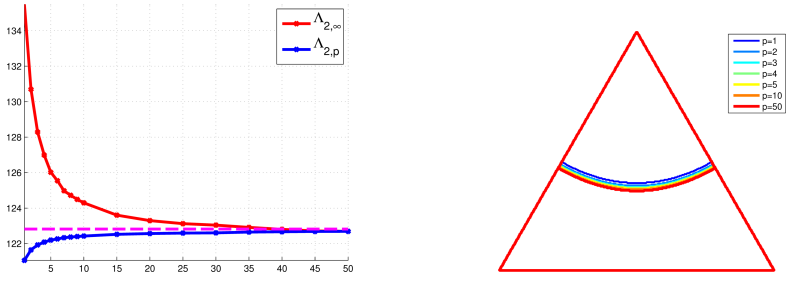

(a) $\Lambda_{2,p}(\mathcal{D}^{2,p})$, $\Lambda_{2,\infty}(\mathcal{D}^{2,p})$ and $\Lambda_2^{DN}(\triangle)$ vs. p (b) $\mathcal{D}^{2,p}$ vs. p

FIGURE 18. p-minimal 2-partitions of the equilateral triangle *vs.* p.

For $k = 3$ we obtain an equipartition starting from $p = 1$ and thus the partition does not change with p and the energies are constant with respect to p. This suggests that the p-minimal 3-partition is given by Figure 6(a) and $p_\infty(\triangle, k) = 1$.

For $k = 4$, since the 4-th eigenvalue of the equilateral triangle is Courant sharp, we know that the minimal 4-partition for $p = \infty$ is the partition with 4 similar equilateral triangles (see Figure 4(b)). The evolution of the partitions according to p is given in Figure 19, where $L_4(\triangle) = \lambda_4(\triangle) = \mathfrak{L}_{4,\infty}(\triangle)$ is plotted in magenta. We observe the convergence of $\Lambda_{k,p}(\mathcal{D}^{k,p})$ as well as the decay of the largest first eigenvalue to $\lambda_4(\triangle)$. The partition $\mathcal{D}^{k,p}$ changes in a significant way with p. Indeed, it seems that the minimal 4-partition for the sum has 4 singular points on the boundary and two inside. The points are moving with p to collapse when $p = \infty$ where we have only 3 singular points on the boundary. Furthermore, the minimal 4-partition for the max has more symmetry than those for $p < \infty$.

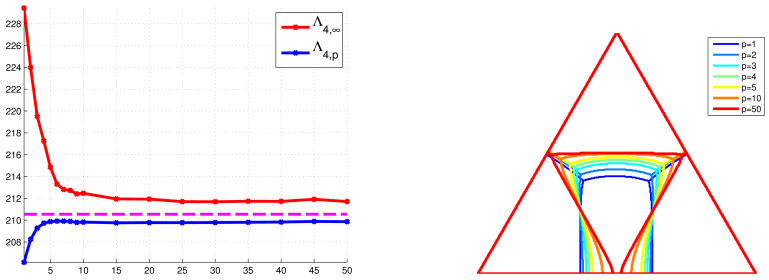

(a) $\Lambda_{4,p}(\mathcal{D}^{2,p})$, $\Lambda_{4,\infty}(\mathcal{D}^{4,p})$ and $\lambda_4(\triangle)$ vs. p (b) $\mathcal{D}^{4,p}$ vs. p

FIGURE 19. p-minimal 4-partitions of the equilateral triangle *vs.* p.

We represent in Figure 20 the evolution of the partitions for these values of k. For $k \in \{5, 7, 8, 9\}$ we observe similar behaviors for the maximal eigenvalue and the p-norm as the ones already shown for $k \in \{2, 4\}$.

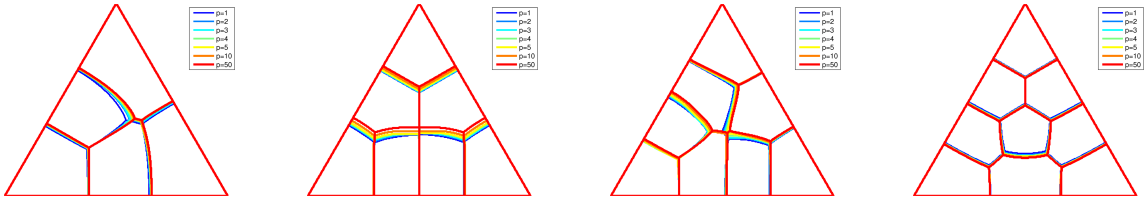

FIGURE 20. p-minimal k-partitions of the equilateral triangle *vs.* p, for $k \in \{5, 7, 8, 9\}$.

The remaining cases $k \in \{6, 10\}$ are in the class of triangular numbers and as observed before (see Figure 17) in these cases it seems that the cells of the optimal partitions are polygonal domains. As seen in the previous section, the L^2 norm criterion does not allow us to say that the candidates found for minimizing $\mathfrak{L}_{k,\infty}$ are not minimizers for $\mathfrak{L}_{k,1}$ in these cases. The study of the evolution of the p-norms does not allow us to conclude that these partitions are different. In fact, the partitions are not observed to move at all and the energies do not vary much. This reinforces the observations at the end of the previous section where we have seen that the partitions minimizing the sum or the maximal eigenvalue are either the same or too close to decide.

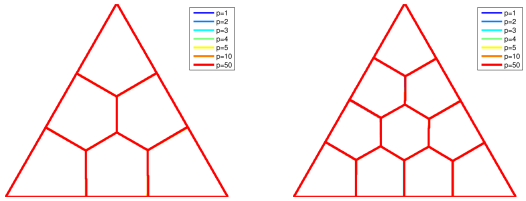

FIGURE 21. p-minimal k-partitions of the equilateral triangle *vs.* p, for $k \in \{6,\ 10\}$.

5.3. **The square.** In cases $k \in \{2, 4\}$ we obtain equipartitions starting from $p = 1$, which makes the energies and partitions stationary (see Figure 4 where we represent the nodal partition associated with the second and fourth eigenfunctions).

For $k = 3$ we have seen in the previous section that there seem to be different p-minimal 3-partitions for $p = 1$ and $p = \infty$. This can also be seen by looking at the evolution of the partitions and of the p-norms in Figure 22. We clearly see how the triple point approaches the center of the square, represented by a black dot in Figure 22.

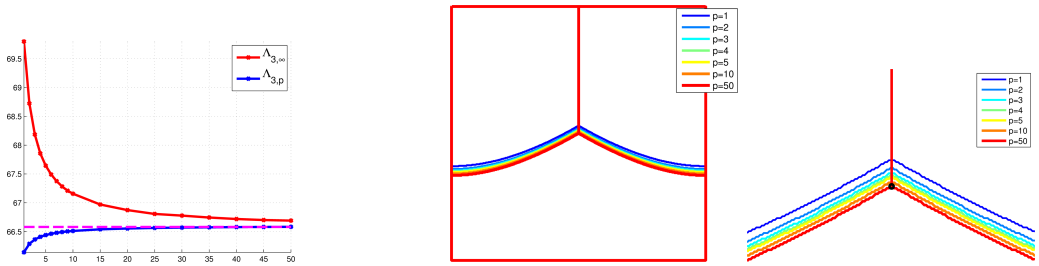

(a) $\Lambda_{3,p}(\mathcal{D}^{3,p})$, $\Lambda_{3,\infty}(\mathcal{D}^{3,p})$ and $\Lambda_3^{DN}(\square)$ vs. p (b) $\mathcal{D}^{3,p}$ vs. p

FIGURE 22. p-minimal 3-partitions of the square *vs.* p.

Another interesting case is $k = 5$. Here we were also able to use a Dirichlet-Neumann approach in order to present an equipartition which is a candidate for minimizing the maximal first eigenvalue. As seen in the previous section the L^2 norm criterion does show that the same partition cannot also be optimal for the sum. We observe in Figure 23 that the energies and the numerical p-minimal 5-partitions evolve when p grows.

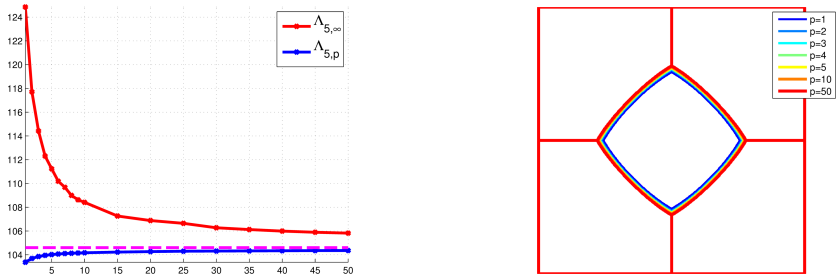

(a) $\Lambda_{5,p}(\mathcal{D}^{5,p})$, $\Lambda_{2,\infty}(\mathcal{D}^{5,p})$ and $\Lambda_5^{DN}(\square)$ vs. p (b) $\mathcal{D}^{5,p}$ vs. p

FIGURE 23. p-minimal 5-partitions of the square *vs.* p.

When $k \in \{6, 8, 9, 10\}$ we observe in Figure 24 similar behaviors in the evolution of the energies and the numerical p-minimal k-partitions.

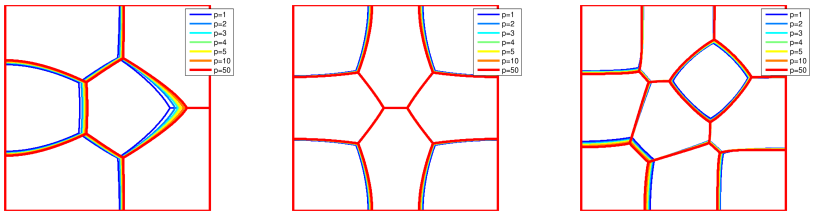

FIGURE 24. p-minimal k-partitions of the square *vs.* p, for $k \in \{6, 8, 10\}$.

We mention that for $k = 9$ the largest eigenvalue of the partition we obtain for $p = 50$ is not smaller than the partition into 9 equal squares. On the other hand, we know that

the partition into 9 equal squares is not optimal for $p = \infty$ since it is a nodal partition which is not Courant sharp (see Proposition 3.6 and [1] for more details). We believe that the partition we obtained for $k = 9$ may have the right structure of the minimizer, but the errors made in the penalized eigenvalue setting make us obtain a slightly higher energy. For reference, the maximal eigenvalue obtained for $p = 50$ is 179.21 (and 178.08 with the penalized method) and the first eigenvalue of a square of side $1/3$ is $L_9(\square) = 177.65$. The evolution of the energies and the numerical 9-partition can be viewed in Figure 25.

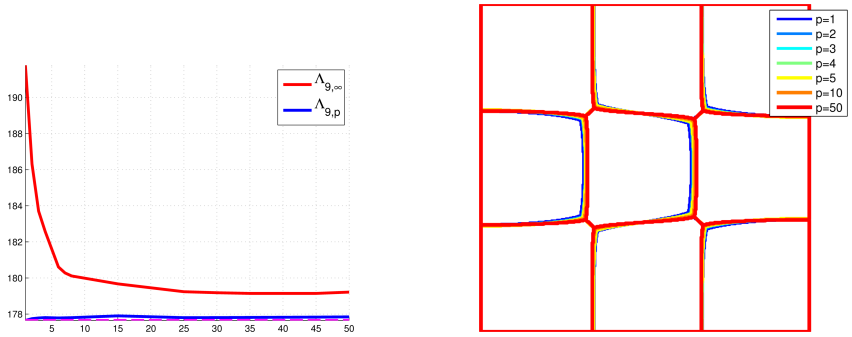

(a) $\Lambda_{9,p}(\mathcal{D}^{9,p})$, $\Lambda_{9,\infty}(\mathcal{D}^{9,p})$ and $L_9(\square)$ vs. p (b) $\mathcal{D}^{9,p}$ vs. p

FIGURE 25. p-minimal 9-partitions of the square *vs.* p.

Something different happens for $k = 7$ where we have two configurations which have close energies at optimum. We represent the partitions of the two configurations in Figure 26 along with a comparison of the maximal eigenvalues and p-norms. We can see that while the first configuration has a lower maximal eigenvalue for large p, the first configuration always has a lower p-norm. We note that when we use the penalization method we find the first configuration which is consistent with the results obtained with the p-norm. We remark that these configurations we obtain are similar to the ones presented in [18]. Still, the small differences we observe for the maximal eigenvalues and the p-norms may be due to our limited numerical precision. In order to conclude which of these partition is better than the other we would need to use some more refined methods which do not use relaxations.

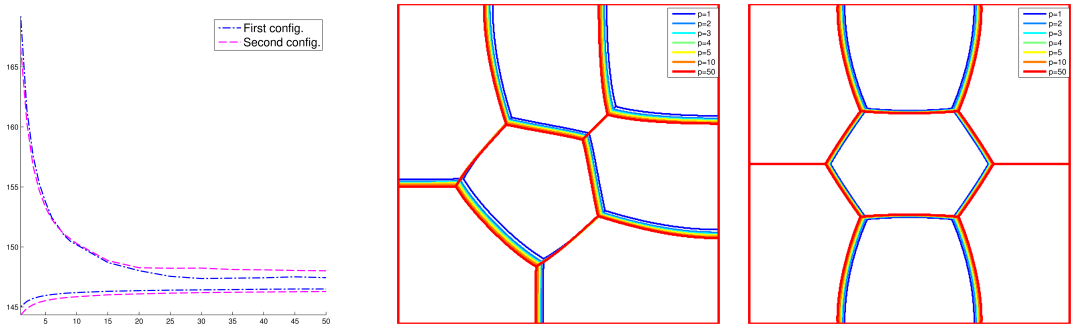

(a) $\Lambda_{k,p/\infty}(\mathcal{D}_j^{5,p})$ vs. p for $j = 1,\ 2$ (b) $\mathcal{D}_1^{5,p}(\square)$ vs. p (c) $\mathcal{D}_2^{7,p}(\square)$ vs. p

FIGURE 26. Comparison of two candidates for 7-partition of the square.

5.4. **The disk.** In this case for $k \in \{2, 3, 4, 5\}$ we obtain numerically that $\mathfrak{L}_{k,p}(\bigcirc)$ is minimized by k equal sectors starting from $p = 1$. In such cases, where we obtain an equipartition when optimizing the sum, the optimal partition is the same for all p and the p-norm does not vary with p. The partitions can be visualized in Figure 2.

In cases $k \in \{6, 8, 9\}$ we obtain for every p partitions consisting of a rounded regular polygon with $k-1$ sides surrounded by $k-1$ equal subsets of a sector of angle $2\pi/(k-1)$. In these cases we may see clearly how the optimal partition evolves with p. For $k \in \{6, 8, 9\}$ we have seen in the end of the previous section that there seem to be different optimal partitions for the sum and for the max. The evolution of the partitions is represented in Figure 27. For $k = 10$ the best candidate is obtained with the iterative method. The evolution of the p-norm of eigenvalue and of the maximal eigenvalue with respect to p is presented in Figure 28. We may see that the candidate found for the sum is not optimal for the max since the maximal eigenvalue strictly decreases with respect to p.

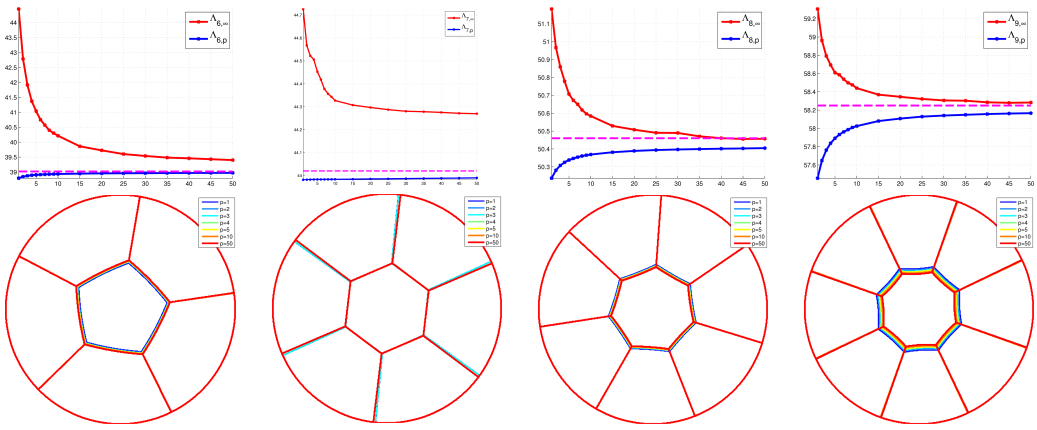

(a) $k = 6$ (b) $k = 7$ (c) $k = 8$ (d) $k = 9$

FIGURE 27. p-minimal k-partitions of the disk *vs.* p, for $k \in \{6, 7, 8, 9\}$.

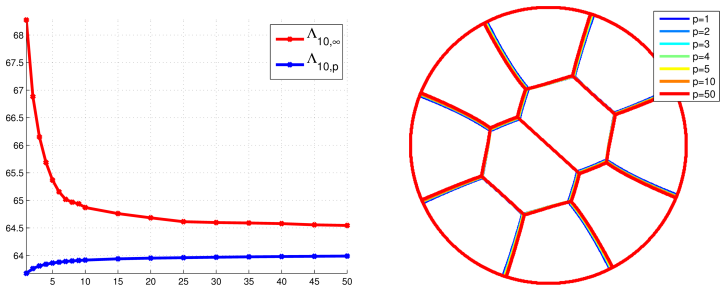

FIGURE 28. p-minimal 10-partitions of the disk *vs.* p.

For $k = 7$ the optimal partition seems to be made out of a regular hexagon and 6 equal sector portions. The partitions and the evolution of the energies is depicted in Figure 27(b). Even if the evolution of the energies and the partitions is not as evident as in the other cases we see that the maximal eigenvalue decreases with p and this seems to indicate, like in the analysis performed at the end of the previous section, that the partitions minimizing the sum and the max are not the same.

5.5. **Conclusion.** We have seen different behaviors according to Ω, k or p. It seems that either the energy $\mathfrak{L}_{k,p}(\Omega)$ is constant with p and there exists a k-partition which is p-minimal for any $p \geq 1$, or the energy $\mathfrak{L}_{k,p}(\Omega)$ is strictly increasing with p. With Definition (3.3), this writes

$$p_\infty(\Omega, k) \in \{1, \infty\}.$$

Numerical simulations suggest (see Conjecture 1.3) that $p_\infty(\Omega, k) = 1$ if

– Ω is a disk and $k \in \{2, 3, 4, 5\}$,

– Ω is a square and $k \in \{2, 4\}$,
– Ω is an equilateral triangle and $k = n(n+1)/2$ with $n \geq 1$.

Acknowledgments. This work was partially supported by the ANR (Agence Nationale de la Recherche), project OPTIFORM, n°ANR-12-BS01-0007-02. The authors thank Michael Floater for suggesting us to look more carefully at k-partitions of the equilateral triangle when k is a triangular number.

References

[1] P. Bérard and B. Helffer. Dirichlet eigenfunctions of the square membrane: Courant's property, and A. Stern's and Å. Pleijel's analyses. In *Analysis and geometry*, volume 127 of *Springer Proc. Math. Stat.*, pages 69–114. Springer, Cham, 2015.
[2] P. Bérard and B. Helffer. Courant-Sharp Eigenvalues for the Equilateral Torus, and for the Equilateral Triangle. *Lett. Math. Phys.*, 106(12):1729–1789, 2016.
[3] P. Bérard and B. Helffer. The weak Pleijel theorem with geometric control. *J. Spectr. Theory*, 6:1–17, 2016.
[4] B. Bogosel and B. Velichkov. A multiphase shape optimization problem for eigenvalues: qualitative study and numerical results. *SIAM J. Numer. Anal.*, 54(1):210–241, 2016.
[5] V. Bonnaillie-Noël and B. Helffer. Numerical analysis of nodal sets for eigenvalues of Aharonov-Bohm Hamiltonians on the square with application to minimal partitions. *Exp. Math.*, 20(3):304–322, 2011.
[6] V. Bonnaillie-Noël and B. Helffer. On spectral minimal partitions: the disk revisited. *Ann. Univ. Buchar. Math. Ser.*, 4(LXII)(1):321–342, 2013.
[7] V. Bonnaillie-Noël, B. Helffer, and T. Hoffmann-Ostenhof. Aharonov-Bohm Hamiltonians, isospectrality and minimal partitions. *J. Phys. A*, 42(18):185203, 20, 2009.
[8] V. Bonnaillie-Noël, B. Helffer, and G. Vial. Numerical simulations for nodal domains and spectral minimal partitions. *ESAIM Control Optim. Calc. Var.*, 16(1):221–246, 2010.
[9] V. Bonnaillie-Noël and C. Léna. Spectral minimal partitions of a sector. *Discrete Contin. Dyn. Syst. Ser. B*, 19(1):27–53, 2014.
[10] V. Bonnaillie-Noël and C. Léna. Spectral minimal partitions for a family of tori. *Exp. Math.*, pages 1–15, 2016.
[11] V. Bonnaillie-Noël, B. Noris, M. Nys, and S. Terracini. On the eigenvalues of Aharonov-Bohm operators with varying poles. *Anal. PDE*, 7(6):1365–1395, 2014.
[12] B. Bourdin, D. Bucur, and É. Oudet. Optimal partitions for eigenvalues. *SIAM J. Sci. Comput.*, 31(6):4100–4114, 2009/10.
[13] D. Bucur and G. Buttazzo. *Variational methods in shape optimization problems*. Progress in Nonlinear Differential Equations and their Applications, 65. Birkhäuser Boston, Inc., Boston, MA, 2005.
[14] D. Bucur, G. Buttazzo, and A. Henrot. Existence results for some optimal partition problems. *Adv. Math. Sci. Appl.*, 8(2):571–579, 1998.
[15] L. A. Cafferelli and F. H. Lin. An optimal partition problem for eigenvalues. *J. Sci. Comput.*, 31(1-2):5–18, 2007.
[16] M. Conti, S. Terracini, and G. Verzini. An optimal partition problem related to nonlinear eigenvalues. *J. Funct. Anal.*, 198(1):160–196, 2003.
[17] M. Conti, S. Terracini, and G. Verzini. On a class of optimal partition problems related to the Fučík spectrum and to the monotonicity formulae. *Calc. Var. Partial Differential Equations*, 22(1):45–72, 2005.
[18] O. Cybulski and R. Hołyst. Tiling a plane in a dynamical process and its applications to arrays of quantum dots, drums, and heat transfer. *Phys. Rev. Lett.*, 95:088304, Aug 2005.
[19] G. Dal Maso and U. Mosco. Wiener's criterion and Γ-convergence. *Appl. Math. Optim.*, 15(1):15–63, 1987.
[20] F. Hecht. New development in FreeFem++. *J. Numer. Math.*, 20(3-4):251–265, 2012.
[21] B. Helffer and T. Hoffmann-Ostenhof. On minimal partitions: new properties and applications to the disk. In *Spectrum and dynamics*, volume 52 of *CRM Proc. Lecture Notes*, pages 119–135. Amer. Math. Soc., Providence, RI, 2010.
[22] B. Helffer and T. Hoffmann-Ostenhof. Remarks on two notions of spectral minimal partitions. *Adv. Math. Sci. Appl.*, 20(1):249–263, 2010.
[23] B. Helffer, T. Hoffmann-Ostenhof, and S. Terracini. Nodal domains and spectral minimal partitions. *Ann. Inst. H. Poincaré Anal. Non Linéaire*, 26(1):101–138, 2009.
[24] A. Henrot. *Shape optimization and spectral theory*. De Gruyter, 2016.
[25] D. Martin. Mélina, bibliothèque de calculs éléments finis. http://anum-maths.univ-rennes1.fr/melina/danielmartin/melina, 2007.

[26] Å. Pleijel. Remarks on Courant's nodal line theorem. *Comm. Pure Appl. Math.*, 9:543–550, 1956.
[27] J. R. Shewchuk. Delaunay refinement algorithms for triangular mesh generation. *Comput. Geom.*, 22(1-3):21–74, 2002. 16th ACM Symposium on Computational Geometry (Hong Kong, 2000).
[28] M. van den Berg and K. Gittins. On the number of courant sharp Dirichlet eigenvalues. arXiv:1602.08376, 2016.

(B. Bogosel) Département de Mathématiques et Applications (DMA - UMR 8553), PSL Research University, ENS Paris, CNRS, 45 rue d'Ulm, F-75230 Paris cedex 05, France
E-mail address: beniamin.bogosel@ens.fr

(V. Bonnaillie-Noël) Département de Mathématiques et Applications (DMA - UMR 8553), PSL Research University, CNRS, ENS Paris, 45 rue d'Ulm, F-75230 Paris cedex 05, France
E-mail address: bonnaillie@math.cnrs.fr